© 2016. Published by The Company of Biologists Ltd | Journal of Cell Science (2016) 129, 4238-4251 doi:10.1242/jcs.191684

RESEARCH ARTICLE

Acid sphingomyelinase is required for cell surface presentation of Met receptor tyrosine kinase in cancer cells

Linyu Zhu[1,2], Xiahui Xiong[2], Yongsoon Kim[2], Naomi Okada[2], Fei Lu[1], Hui Zhang[2] and Hong Sun[2,*]

ABSTRACT

Receptor tyrosine kinases (RTKs) are embedded in the lipid bilayer of the plasma membrane, but the specific roles of various lipids in cell signaling remain largely uncharacterized. We have previously found that acid sphingomyelinase (ASM; also known as SMPD1) regulates the conserved DAF-2 (the ortholog IGF-1R in mammals) RTK signaling pathway in *Caenorhabditis elegans*. How ASM and its catalytic products, ceramides, control RTK signaling pathways remain unclear. Here, we report that ASM regulates the homeostasis of Met, an RTK that is frequently overexpressed in various cancers. Inactivation of ASM led to a rapid loss of Met from the plasma membrane, reduced Met phosphorylation and activation, and induced Met accumulation in the trans-Golgi network (TGN). However, trafficking of integrin β3 and vesicular stomatitis virus glycoprotein (VSVG) was largely unaffected. Knockdown of syntaxin 6 (STX6) also blocked the Golgi exit of Met. Depletion of either ASM or STX6 led to aberrant trafficking of Met to lysosomes, promoting its degradation. Our studies reveal that ASM and ceramides, together with STX6 and cholesterol, constitute a new regulatory mechanism for the exit of Met from the Golgi during its biosynthetic route, which is used to rapidly replenish and regulate the plasma membrane levels of Met in various cancer cells.

KEY WORDS: Acid Sphingomyelinase, ASM, Syntaxin 6, STX6, Met, Ceramide, Golgi, SMPD1, Receptor tyrosine kinase, RTK

INTRODUCTION

The *Met* (also called c-Met) proto-oncogene encodes a receptor tyrosine kinase (RTK) that is expressed in epithelial cells of many organs, including pancreas, kidney, liver, bone marrow and muscle. Activation of the Met RTK by its cognate ligand, hepatocyte growth factor (HGF), triggers mitogenesis and morphogenesis, and is essential during embryonic development, cell migration, wound healing and angiogenesis (Maroun and Rowlands, 2014). The expression of Met is aberrantly upregulated in many human malignancies, including glioblastoma (GBM) (Koochekpour et al., 1997), which is the most aggressive and therapeutically difficult brain tumor (Maher et al., 2001; Stommel et al., 2007). Abnormal activation of Met is responsible for resistance to targeted therapies against vascular endothelial growth factor receptor (VEGFR) in GBM and inhibitors of the epithelial growth factor receptor (EGFR) in lung cancers (Engelman et al., 2007; Lin and Bivona, 2012).

[1]School of Chemical Biology and Biotechnology, Peking University Shenzhen Graduate School, Shenzhen, Guangdong 518055, China. [2]Department of Chemistry and Biochemistry, University of Nevada, Las Vegas, NV 89135, USA.

*Author for correspondence (Hong.sun@unlv.edu)

H.S., 0000-0003-2100-1451

Received 3 May 2016; Accepted 30 September 2016

Upon the binding to its cognate ligand, HGF, Met is phosphorylated and activated on the plasma membrane. The activated Met is subsequently endocytosed and targeted by ubiquitin-dependent sorting to the lysosomal degradation pathway (Clague, 2011; Jeffers et al., 1997). Certain activating mutations in the kinase domain of Met, originally identified in human renal papillomas, allow the receptor to constitutively recycle back to the cell surface, leading to aberrant Met activation and tumorigenesis (Clague, 2011; Joffre et al., 2011). The net levels of many RTKs on the plasma membrane are also maintained through the continued replenishment with the newly synthesized receptor proteins derived from the Golgi (Clague, 2011). For example, the Golgi exit of an RTK, VEGFR, is shown to be regulated by its ligand VEGF in endothelial cells (Manickam et al., 2011).

RTKs are lipid-embedded proteins in the membranes, but the specific roles of various lipids and their regulation by lipid enzymes during RTK-mediated cell signaling remain largely unclear. Recent research by our laboratory and others indicates that the proper signaling of RTKs is further regulated by dynamic properties of the membrane itself. In particular, the enzyme acid sphingomyelinase (ASM; also known as SMPD1) catalyzes the hydrolysis of sphingomyelin to produce ceramide and phosphocholine (Jenkins et al., 2009). Germline mutations in the human *ASM* gene are responsible for Niemann Pick type A disease, and affected individuals exhibit severe degeneration of Purkinje neurons and death at young ages (Schuchman, 2007). A variety of stress stimuli activate ASM, which is found on the outer leaflet of the plasma membrane, to promote the formation of unique lipid entities on the plasma membrane, the hypothesized ceramide-enriched lipid rafts (Cremesti et al., 2001; Grassme et al., 2001; van Blitterswijk et al., 2003). Lipid rafts are plasma membrane microdomains that are enriched in cholesterol and sphingomyelin (Lingwood and Simons, 2010; Rajendran and Simons, 2005). Ceramide lipids have an inherent biophysical property of self-association and aggregation, which could promote protein–protein or protein–lipid interactions (van Blitterswijk et al., 2003). However, the physiological function of ASM in mammalian cells is unclear. Our laboratory has recently identified the worm ASM homolog, ASM-3, as a new and positive regulator of the conserved DAF-2 (IGF-1R-like) signaling pathway in *Caenorhabditis elegans* (Kim and Sun, 2007, 2012). Here, we report our new findings on the role of ASM in regulating the Met cell surface levels and downstream signaling in human GBM cells.

RESULTS

Inactivation of ASM reduces the levels of the tyrosine-phosphorylated Met protein

To understand ASM function in mammalian cells, we searched various databases for ASM expression profiles and found that ASM is highly expressed in cancer cell lines derived from melanoma, breast cancer and especially GBM (Fig. S1A). To investigate the potential involvement of ASM in cell signaling in GBM cells, we

Journal of Cell Science

Journal of Cell Science (2016) 129, 4238-4251 doi:10.1242/jcs.191684

initially focused on the potential effects of ASM inactivation on Met, an RTK that is often highly expressed in GBM. Knockdown of ASM by using two independent small interfering (si)RNAs in U373 glioblastoma cells caused a marked reduction of the activation-associated form of Met that is phosphorylated at residues Y1234 and Y1235, whereas total Met protein levels were only modestly decreased (Fig. 1A, top panel and quantified in D).

As siRNA-mediated knockdown of ASM usually achieved about 80–95% reduction of ASM protein in 48–72 h (Fig. 1A, bottom panel and quantified in C, bottom panel); we also used desipramine, a functional chemical inhibitor of ASM known to interfere in the interaction of ASM with lipids in lysosomes to promote rapid ASM protein degradation (Jaffrezou et al., 1995; Jenkins et al., 2011). Indeed, desipramine treatment rapidly destabilized the ASM protein (Fig. 1C, top panel and quantified in C, bottom panel) and consequently downregulated levels of tyrosine-phosphorylated Met and of phosphorylated RPS6KB1 (S6K) in U373-MG and several other GBM cell lines (Fig. 1B,E). Our studies thus revealed that ASM is required to maintain the steady-state levels of the tyrosine-phosphorylated Met protein in GBM cells.

ASM is required for the plasma membrane association of Met but not of integrin β3

Because phosphorylated Met usually represents its activated form on the plasma membrane, we examined the distribution of Met by immunostaining (Fig. 2). In control cells, Met was readily detected on the plasma membrane and in a diffuse pattern at perinuclear regions (Fig. 2A). Immunostaining was specific for Met given that knockdown of Met by two independent siRNAs greatly eliminated both the plasma membrane and intracellular staining (Fig. S1C). The Met staining on the plasma membrane was greatly diminished by desipramine or by knockdown of ASM with two specific siRNAs, whereas its intracellular staining became more discrete and focused around the perinuclear region (Fig. 2A,B). Analysis using a linescan function with the onboard microscope software confirmed these assessments (Fig. 2A, fluorescence intensity profiles). As

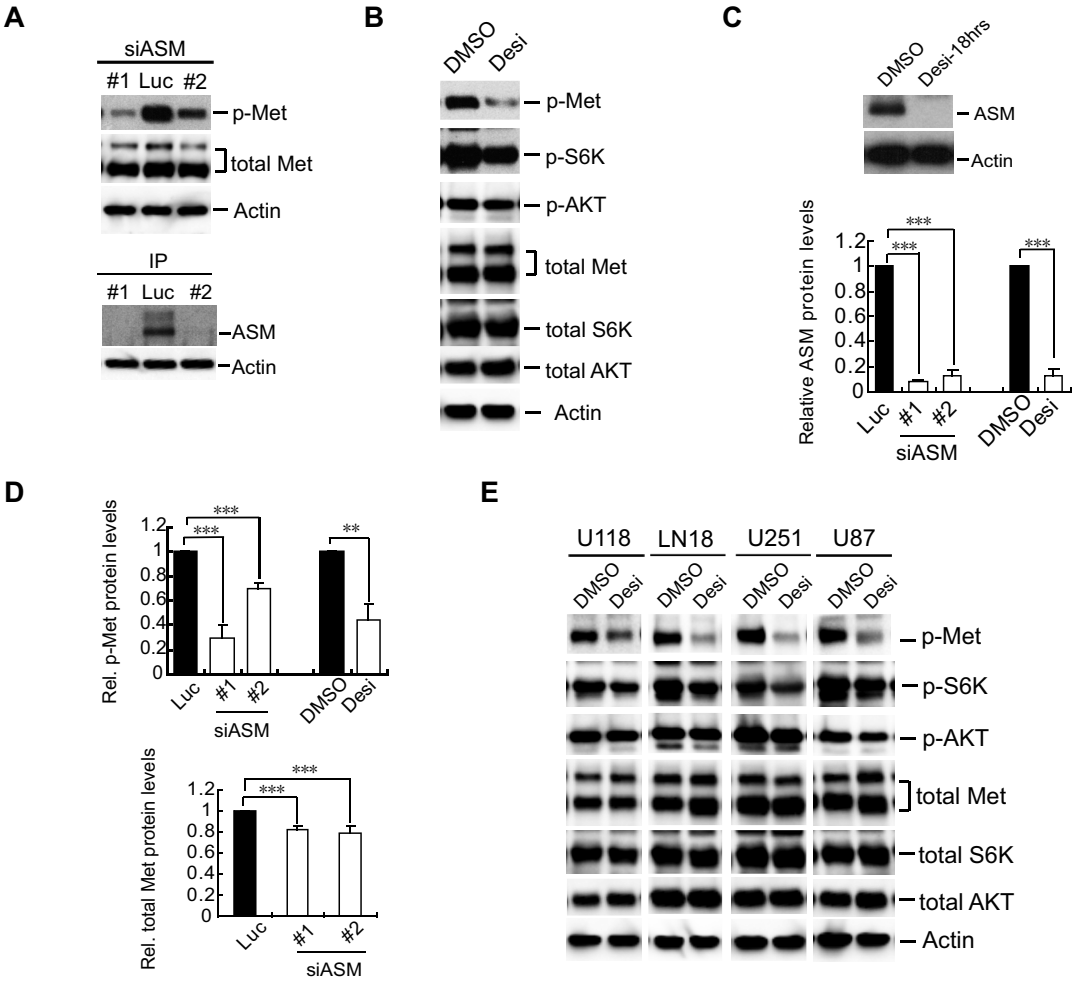

Fig. 1. Inactivation of ASM reduces the levels of tyrosine-phosphorylated Met. (A) U373-MG cells were transfected with an siRNA against luciferase (Luc, control) or two independent siRNAs against ASM (#1 and #2; siASM). Lysates harvested at 72 h post transfection were analyzed by immunoblotting with antibodies for Y1234- and Y1235-phosphorylated Met (p-Met) and total Met (upper band, p170; lower band, p145) with actin as a loading control. (B) U373-MG cells were treated with DMSO (control) or 30 µM desipramine (Desi) for 18 h. Membranes were immunoblotted for the indicated proteins. p-, phosphorylated. (C) Changes in ASM protein levels were examined by immunoprecipitation and western blotting analyses with anti-ASM antibodies, with equal amounts of lysates, using actin as the control. Bottom, a quantification of ASM proteins in the ASM-inactivated cells from panels A and C, normalized to values from control cells, with the mean and error bars (s.d.) from three independent repeats (statistical significance, ***P<0.001). (D) A quantification of the relative (Rel.) intensities of tyrosine-phosphorylated Met (p-Met) as to the total Met protein (top) and of the changes in the amount of total Met protein normalized to the actin loading control in control and ASM-inactivated cells in panels A and B (***P<0.001 and **P<0.01, Student's t-test). (E) The GBM cell lines U118-MG (U118), LN18, U251-MG (U251) and U87-MG (U87) were each treated with DMSO or 30 µM of desipramine, and membranes were immunoblotted for the indicated proteins as in panel B.

Journal of Cell Science (2016) 129, 4238-4251 doi:10.1242/jcs.191684

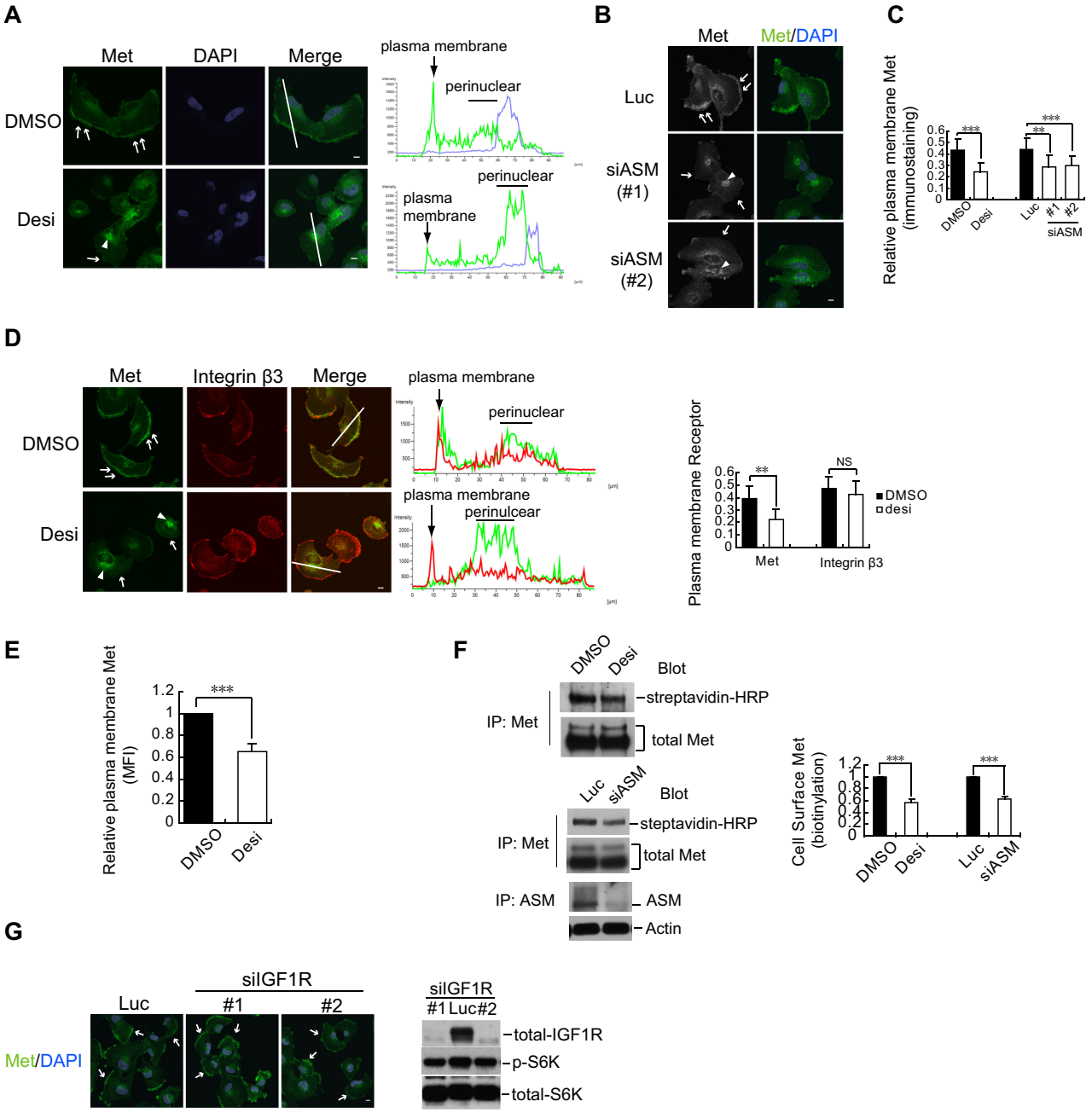

Fig. 2. Inactivation of ASM triggers loss of Met from the plasma membrane and causes its intracellular accumulation. (A) U373-MG cells were treated with DMSO (control) or 30 µM desipramine (Desi) for 18 h. Cells were immunostained and examined by confocal microscopy with antibodies for Met (green), and DAPI (blue) as a nuclei counter-stain. Arrows, Met on plasma membrane; arrowheads, intracellular Met staining. Linescan intensity profiles show the green and blue fluorescence intensities (*y*-axis, arbitrary units) along the white line drawn across the cell (*x*-axis, distance in µm). Arrow on linescan indicates position of the plasma membrane. (B) U373-MG cells were treated with control siRNA (Luc) or two independent siRNAs against ASM (#1 and #2; siASM) for 72 h. Cells were immunostained as described in panel A. Arrows, Met on plasma membrane; arrowheads, intracellular Met staining. (C) The means of the cell plasma membrane Met intensities in control and ASM-inactivated cells were compared (error bars indicate s.d.), obtained by quantifying Met staining in the plasma membrane region versus that in the whole cell (about 100 cells from three independent experiments were measured for each condition, statistical significance ***P<0.001 and **P<0.01, Student's *t*-test). (D) Cells, treated as described in panel A, were immunostained, examined with antibodies for Met (green) and integrin β3 (red), and the relative plasma membrane fluorescence intensities of Met or integrin β3 were quantified as described in panel C (statistical significance: ***P<0.001; NS, not significant; Student's *t*-test). Arrows, Met on plasma membrane; arrowheads, intracellular Met staining. Arrow on linescan indicates position of the plasma membrane. (E) U373-MG cells were treated with DMSO or desipramine. Live cells were detached using a mild protease and processed for surface staining with an anti-Met antibody, and then analyzed by using FACS on triplicate experiments (statistical significance: ***P<0.001, Student's *t*-test). Relative plasma membrane Met was determined by measuring the mean fluorescence intensities (MFIs). (F) Cells were treated with DMSO or desipramine as in A, or with control siRNA (Luc) or ASM siRNAs (oligonucleotide #1, siASM) as in B. Subsequently, attached live cells were then briefly labeled with biotin and lysed, and Met proteins were immunoprecipitated (IP) with anti-Met antibodies. The surface-biotinylated Met was detected with streptavidin–HRP, compared and quantified relative to total Met analyzed by using anti-Met antibodies (quantification from three independent experiments, right). (G) U373-MG cells were transfected with control siRNA (Luc) and two independent siRNAs against IGF-1R (#1 and #2; siIGF1R), fixed 72 h later, and analyzed by immunostaining with an anti-Met antibody or by western blotting for the indicated proteins. p-, phosphorylated. Scale bars: 10 µm (A,B,D,G).

Journal of Cell Science (2016) 129, 4238-4251 doi:10.1242/jcs.191684

measured and quantified in ~100 cells from three independent experiments, the relative plasma membrane Met fluorescence intensity was reduced by 40–50% in the ASM-knockdown cells (Fig. 2C).

To determine whether the effect of ASM inactivation is specific for Met, we examined the cellular distribution of integrin β3, another plasma membrane protein. Differentially labeled antibodies against Met and integrin β3 in double-immunostaining analyses revealed that only Met, not integrin β3, was lost from the plasma membrane and accumulated in the intracellular compartments after desipramine treatment (Fig. 2D). These observations indicate that ASM selectively regulates the plasma membrane localization of Met, but not that of integrin β3.

We also quantitatively analyzed the cell-surface-associated Met proteins in live cells by using fluorescence-activated cell sorting (FACS) (Fig. 2E; Fig. S1B). These FACS analyses showed that there was ~40% reduction in the amount of cell-surface-associated Met in the desipramine-treated cells, as compared to that in controls. In addition, we also measured the plasma membrane Met by using a cell surface biotinylation method (Roberts et al., 2001). Attached cells were exposed to a brief reaction with sulfo-NHS-LC-biotin to label cell surface proteins, cells were then lysed, and Met proteins were immunoprecipitated with antibodies against Met, followed by immunoblotting analysis with streptavidin-conjugated horseradish peroxidase (HRP) to detect the biotinylated Met proteins. Such studies showed that inactivation of ASM by either desipramine or siRNAs against ASM each reduced the amount of Met at the cell surface by ~40% (Fig. 2F, and quantified in the right panels), consistent with the results from the immunostaining studies and FACS analysis. Taken together, our studies indicate that ASM regulates the levels of plasma-membrane-associated Met, but not those of integrin β3, and that ASM inactivation traps Met in discrete intracellular compartments.

ASM regulates Met distribution independent of IGF-1R

Because we initially identified the worm ASM homolog as a new regulator of the conserved DAF2 (IGF-1 receptor-like) signaling pathway in *Caenorhabditis elegans* (Kim and Sun, 2007, 2012), we wondered whether the effects of ASM inactivation on Met localization are mediated through the inhibition of the IGF-1R signaling pathway in GBM cells. We therefore silenced the IGF-1R gene using two independent siRNAs, which almost completely abolished the expression of the IGF-1R gene (Fig. 2G). However, loss of IGF-1R did not affect the plasma membrane localization of Met (Fig. 2G), suggesting that regulation of plasma-membrane-associated Met by ASM is independent of ASM regulation of IGF-1R.

Loss of ASM leads to accumulation of Met in the Golgi compartment

To determine whether Met accumulated in specific organelles after ASM inactivation, we tried to co-immunostain Met with several organelle-specific markers. Our analyses revealed that the main intracellular region(s) in which Met accumulated in ASM-deficient cells were marked by several Golgi-specific markers, especially the areas marked by p230 (also known as Golgin-245 and GOLGA4) (Fig. 3A,B). p230 is a coiled-coil protein with characteristic localization in the trans-Golgi network (TGN) compartment (Gleeson et al., 2004). Fluorescence intensity linescan analyses of Met and p230 immunostainings also confirmed that the increased intracellular Met staining overlapped with that of p230 in cells that had been treated with desipramine or siRNAs against ASM (Fig. 3A,B). Quantification of the staining of Met in 100 cells to obtain the mean fluorescence intensity of Met in the Golgi further supported this notion (Fig. 3C). Notably, if cells were first treated with an siRNA against ASM, but not if they were transfected with control siRNA, treatment with desipramine no longer induced changes in the Met distribution (Fig. S1D), suggesting that both desipramine and siRNAs against ASM affected ASM in these cells.

Temporal studies of Met distribution revealed that Met started to accumulate in the intracellular regions marked by p230 within 3 h after desipramine treatment, and staining of Met at the plasma membrane was still detectable at this time point; however, Met was no longer detectable at the plasma membrane after 18 h of drug treatment (Fig. 3A, right panel). Similarly, although siRNA-mediated knockdown of ASM was only partial at 24 h, intracellular accumulation of discrete sites of Met staining in the p230-marked-TGN region was readily noticeable (Fig. 3B, top panel), with residual plasma membrane-associated Met staining in some cells that was further reduced at 72 h post-transfection (Fig. 3B, bottom panel).

We also tried to colocalize the intracellular Met with GM130, a cis-Golgi matrix protein, in the desipramine-treated cells (Fig. 3D). Our studies showed that there is partial overlap between Met and GM130 staining, and this overlap appeared to be less perfect than that between Met and p230 (comparing Fig. 3A,D). Double immunostaining of p230 and GM130 also revealed that although both markers were still found in close proximity with each other under both conditions, the extent of their colocalization appeared to be less in the desipramine-treated cells than that in the control cells, raising the possibility that there is a subtle structural change in the TGN in response to desipramine (Fig. 3D).

Although Met initially accumulated in the TGN after ASM knockdown (Fig. 3B), we noticed that after treatment with siRNA against ASM for 72 h, Met also accumulated in the intracellular compartment marked by LAMP2 (Fig. 3E), a lysosome-specific protein marker (Akasaki et al., 1996). Such colocalization was more pronounced at 72 h (Fig. 3E) as compared with that at 24 h post transfection (Fig. S2A), raising the possibility that ASM inactivation leads to the aberrant trafficking of Met to lysosomes for degradation. To test this hypothesis, we treated cells with bafilomycin A1, which blocks the protein degradation activity in lysosomes by inhibiting the vacuolar-type H^+-ATPase (Yoshimori et al., 1991). We found that bafilomycin A1 treatment substantially enhanced the colocalization of Met with LAMP2, and such an effect was much more pronounced in the siRNA-treated cells than that in the control cells (Fig. 3F). Quantification of 70 cells to determine the mean fluorescence intensity of Met staining in the lysosome region further supported this notion (Fig. 3F, right panel). Similar results were obtained when other lysosomes markers, such as CD63 (Fig. 3G) or LAMP1 (Fig. S2B–D), were used. When cells were stained with LysoTracker, a fluorescent dye that stains acidic compartments such as lysosomes in live cells, Met staining also colocalized with that of LysoTracker in the siRNA-treated cells (Fig. S2E). However, because bafilomycin A1 almost completely abolished uptake of the LysoTracker dye owing to inhibition of the lysosome vacuolar-type H^+-ATPase activity, we therefore could not use LysoTracker to quantitatively measure the accumulation of Met in lysosomes in the bafilomycin-A1-treated cells (Fig. S2F). These results suggest that ASM inactivation leads to an increased accumulation of Met in the TGN, accompanied by loss of Met from the plasma membrane. Prolonged trapping of Met in the TGN might subsequently induce aberrant trafficking of the receptor to lysosomes, promoting its eventual degradation.

Journal of Cell Science (2016) 129, 4238-4251 doi:10.1242/jcs.191684

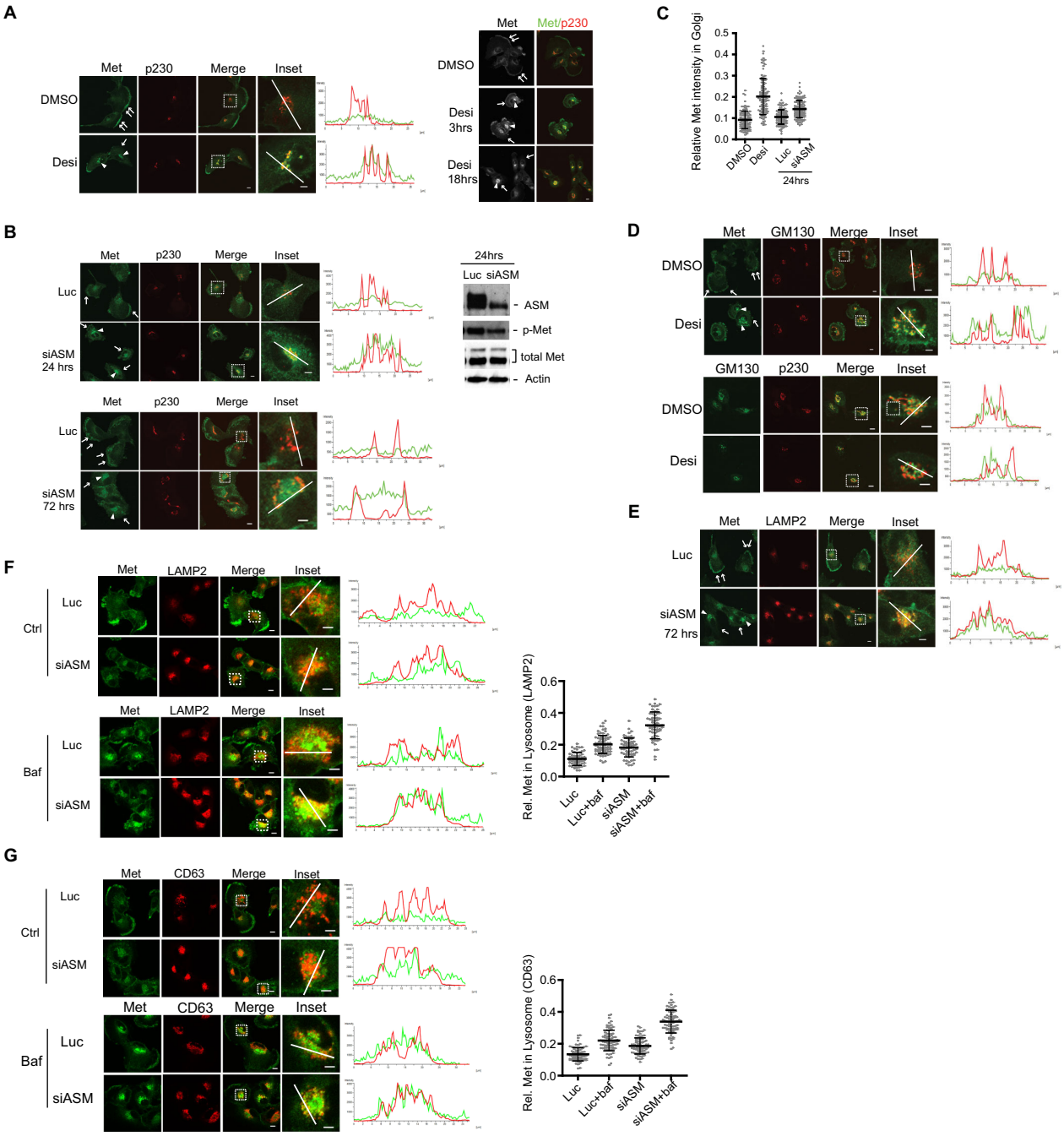

Fig. 3. ASM inactivation leads to Met accumulation in the Golgi compartment. (A) U373-MG cells were treated with DMSO or 35 µM desipramine (Desi) for 3 h. Cells were co-immunostained with antibodies for Met (green) and p230 (red) (left images, arrows: plasma-membrane-associated Met; arrowheads: intracellular Met). Merged channel shows colocalization (yellow) of Met and p230. Insets: enlarged images of the boxed regions. Linescan intensity profiles of green and red fluorescence intensities show colocalization of Met (green) and p230 (red) in the desipramine-treated cells along the white lines. Linescan: *y*-axis, arbitrary units of intensity along the white line drawn across the cell (*x*-axis, distance in µm). Right panel: time course analysis of Met staining after various periods of desipramine treatment. Met started to accumulate in the intracellular perinuclear regions (arrowheads) within 3 h and then was lost from the plasma membrane (arrows) 18 h after desipramine treatment. (B) Cells were transfected with siRNA against Luciferase (Luc) or siRNA against ASM (siASM, #1), and processed 24 or 72 h later for co-immunostaining, as described in panel A. Cell lysates were prepared and examined by western blot analysis with the indicated antibodies, as described in Fig. 1A. (C) Quantification of relative Met staining in the Golgi region. The intensity of Met staining in the Golgi region (marked by p230 staining) relative to the intensity of total Met in the whole cell was measured in 100 cells under each condition (from three independent experiments) and is shown in a scatter plot (mean and s.d. are indicated by the center and vertical bars, respectively). (D,E) Cells, treated as indicated, were processed for co-immunostaining for the indicated proteins. Arrows, Met on plasma membrane; arrowheads, intracellular Met staining. (F,G) Cells were treated with control (Luc) or siRNA against ASM (siASM, #1) for 52 h and then treated with bafilomycin A1 (Baf, 100 nM) for an additional 7 h. Cells were co-immunostained with antibodies against Met and LAMP2 (F) or Met and CD63 (G). Right panels, quantification results of relative (Rel.) Met staining in the LAMP2- or CD63-marked lysosome regions as compared to the intensity of Met staining across whole cells (from about 70 cells for each condition, from three independent experiments) are shown as scatter plots. Scale bars: 10 µm (all images excluding insets); 5 µm (inset images).

Journal of Cell Science (2016) 129, 4238-4251 doi:10.1242/jcs.191684

ASM inactivation induces the rapid turnover of newly synthesized Met protein

To test whether ASM deficiency affects the protein stability of Met, we conducted pulse–chase experiments to measure the protein half-life of Met. Control and ASM-knockdown cells were pulse-labeled with ^{35}S-methionine for 1 h, washed, and incubated in fresh medium (chase) for various times. The newly synthesized Met protein is initially translated as a 170 kDa precursor before it is proteolytically processed in the Golgi to yield mature p45 (α) and p145 (β) subunits (Komada et al., 1993). We used an antibody specific for the C-terminus of Met to detect both the p170 precursor and p145 β subunit of Met proteins (Fig. 4A). We found that during 1 h of labeling with ^{35}S-methionine, Met proteins were primarily synthesized as the precursor p170, with a small amount of mature p145. During the chase period, the majority of p170 was converted into the mature p145 form in control cells (Fig. 4A). In the cells that had been treated with siRNA against ASM, although the rate of conversion of the ^{35}S-labeled precursor p170 to p145 was similar to that of control during the chase period, the half-life of the ^{35}S-labeled p145 Met protein was reproducibly found to be reduced (Fig. 4A; Fig. S3A,B). Consistently, there was also less ^{35}S-labeled p145 upon short exposures of cells to desipramine, whereas small accumulations of p170 were observed in some experiments (Fig. 4A, lower right panel). Western blotting showed that brief treatment with desipramine induced a slight but visible accumulation of p170 Met precursor in cells (Fig. 4C, arrow), while the levels of phosphorylated Met were reduced but the total levels of p145 Met remained relatively constant.

To investigate whether the biosynthesis of Met protein forms an ASM-regulated mechanism to maintain the levels of plasma-membrane-associated Met, we examined the Met response to the protein synthesis inhibitor cycloheximide. We found that cycloheximide effectively inhibited the synthesis of new Met protein, as revealed by the rapid loss of the p170 precursor protein, whereas levels of the total Met protein were modestly affected (Fig. 4B). Immunostaining studies revealed that desipramine-induced accumulation of Met in the Golgi was almost completely abolished by co-treatment with cycloheximide, whereas levels of p230 were not sensitive to cycloheximide (Fig. 4D). Quantification of the fluorescence intensity of staining of Met and p230 at the Golgi in 100 cells to determine the mean values further supports this notion (Fig. 4D, right panel).

If one effect of ASM inactivation is the blocking of the transit of newly synthesized Met through the Golgi, inhibition of the Golgi-mediated Met supply should reduce the cell surface level of Met, as the plasma-membrane-associated Met proteins are continuously internalized through endocytosis after the activation of the receptor. We used brefeldin A (BFA) to test this hypothesis. BFA can specifically disrupt the Golgi network structure and consequently block the trafficking of newly synthesized proteins from ER to Golgi (Klausner et al., 1992). BFA, however, only marginally affects recycling (Lippincott-Schwartz et al., 1991; Miller et al., 1992). We used BFA to examine the relative contribution of the Golgi and recycling routes of Met trafficking. Notably, BFA effectively reduced the amount of plasma-membrane-associated Met and simultaneously caused Met intracellular accumulation, presumably in the ER region (Fig. 4E). BFA also effectively induced p170 accumulation and reduced the cell surface and phosphorylated Met levels in various GBM cells (Fig. 4F; Fig. S3C,D). These observations suggest that the continuous supply of Met from Golgi is an important determinant of the cell surface level of Met.

ASM inhibition does not affect the Golgi transport of the VSVG cargo protein

The requirement for ASM in the trafficking of the newly synthesized Met protein in the Golgi suggests that ASM controls either a general transport function of the Golgi or a specific transport activity of the Golgi for a selective group of cargos, including Met. To distinguish these two possibilities, we examined whether ASM is required for the transport of a vesicular stomatitis virus glycoprotein (VSVG) fusion protein (VSVG-ts045–GFP), a model cargo used to study the protein transport processes between the ER, Golgi and plasma membrane (Hirschberg et al., 1998; Presley et al., 1997). VSVG-ts045 is a viral protein carrying a temperature sensitive mutation that allows the protein to be trapped in ER owing to unfolding at the non-permissive temperature (40°C). At the permissive temperature (32°C), the protein folds normally and transits from ER to Golgi, and then proceeds to the plasma membrane.

To examine the effects of ASM loss on VSVG transport, the cells expressing the VSVG-ts045–GFP mutant were initially cultured at 40°C to trap the newly synthesized VSVG protein in ER. The cells were then shifted to the permissive temperature, 32°C, to allow VSVG to enter into the Golgi (Fig. 5A,B). Our time course analysis revealed that 45 min after temperature shift, VSVG entered the TGN, which can be co-stained with p230 (Fig. 5B). The VSVG mutant protein continued to exit the Golgi and moved further towards the plasma membrane 90–180 min after temperature shift in both control and ASM-knockdown cells (Fig. 5B). Quantification of 50 cells (from three experiments) under each condition revealed similar kinetics for the Golgi exit of the VSVG protein between the control and ASM-knockdown cells (Fig. 5C), suggesting that ASM loss does not prevent the transport of VSVG from Golgi to the plasma membrane. We also used the cell surface biotinylation method to examine the plasma-membrane-associated VSVG to determine the rate of Golgi exit of VSVG. The cell surface VSVG was labeled through a brief exposure of the attached cells to a biotinylation reaction at various times after temperature shift, which was followed by immunoprecipitation with an antibody against VSVG. The cell surface levels of VSVG were analyzed by immunoblotting with streptavidin–HRP (Fig. 5D, upper panel; quantified in Fig. 5E, left panel). These experiments, again, showed that knockdown of ASM did not delay the Golgi exit of VSVG.

STX6 is required for Met trafficking from the Golgi to the cell surface

STX6, a vesicle transport protein in the targeting (t-)SNARE family, is primarily localized in the TGN and partially localized on endosomes. STX6 is required for the Golgi transport of selective cargo proteins, such as VEGFR, GM1 ganglioside and a GFP-tagged glycosylphosphatidylinositol (GPI) fusion protein, but not of VSVG (Choudhury et al., 2006; Manickam et al., 2011). In U373-MG cells, we found that STX6, similar to ASM, was not required for VSVG transport (Fig. 5B–E).

We questioned whether STX6 is involved in the ASM-mediated regulation of Met. In the cells that had been treated with the ASM inhibitor desipramine or siRNAs against ASM, we found that STX6 became more concentrated and colocalized with Met and p230 in the TGN (Fig. 6A). Short periods of silencing of STX6 by using siRNAs (24 h) reduced the Met levels on the plasma membrane and induced the accumulation of Met in the p230-marked TGN (Fig. 6B, top panel). Longer periods of silencing of STX6 (72 h) led to the complete loss of plasma-membrane-associated Met, accompanied by a partial accumulation of Met in the TGN (Fig. 6B, bottom panel). Loss of STX6 also reduced the levels of the surface Met protein, as

Journal of Cell Science (2016) 129, 4238-4251 doi:10.1242/jcs.191684

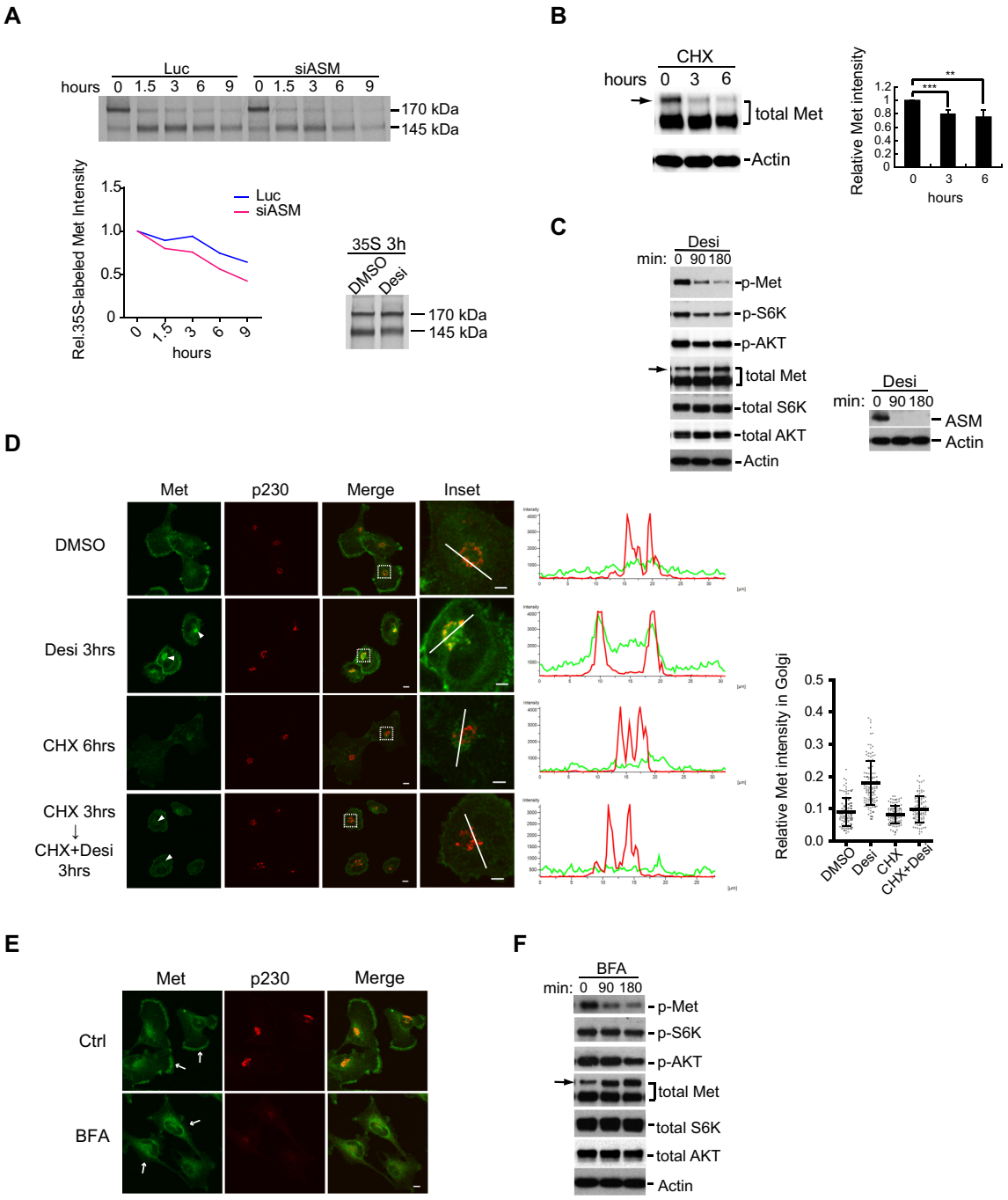

Fig. 4. Biosynthetic Met protein is regulated by ASM. (A) U373-MG cells were transfected with control siRNA and siRNA against ASM (siASM; #1) for 72 h. Cells were pulse-labeled with ^{35}S-labeled methionine for 1 h, washed and chased for various time points as indicated. Met proteins were immunoprecipitated with anti-Met antibodies, resolved in a protein gel and visualized by using fluorography (top panel) and then quantified relative (Rel.) to the Met intensity at 0 hour (bottom left panel). Bottom right, cells were treated with DMSO or 35 µM desipramine (Desi) for 30 min, labeled with ^{35}S-labeled methionine for 3 h in the presence of DMSO or desipramine, and then directly lysed and analyzed. (B) Cells were treated with cycloheximide (100 µg/ml) for 3 or 6 h, and whole cell lysates were immunoblotted with antibodies against Met that recognize both Met precursor (p170, arrow) and the mature β p145 Met protein (lower band). Quantification of p145 Met in response to cycloheximide was plotted (**P<0.01; ***P<0.001; Student's t-test, three independent experiments) with the mean and error bars (s.d.) obtained from three independent repeats. (C) Cells were treated with DMSO or 35 µM desipramine for 90 or 180 min. Cell lysates were split into two portions; one portion was directly examined by immunoblotting analysis for Met and the other indicated proteins (left panel), whereas the other portion was subjected to immunoprecipitation and then western blot analysis for ASM (right panel). Actin was used as control for both panels. p-, phosphorylated protein. (D) Cells were pre-incubated with or without cycloheximide (100 µg/ml) for 3 h. DMSO (control) or 35 µM desipramine (Desi) was then added in the presence or absence of cycloheximide for an additional 3 h. Cells were co-immunostained for Met and p230, and quantified to obtain the means for the relative intensities of Met staining in Golgi regions under various conditions, conducted as described in Fig. 3C. Linescan intensity profiles show the fluorescence intensities (y-axis, arbitrary units) along the white line drawn across the cell (x-axis, distance in µm). Arrowheads, Met staining in the Golgi region. (E) Cells were treated with brefeldin A (BFA, 3 µg/ml) for 3 h and cells were co-stained for Met and p230. Ctrl, control, DMSO. Arrows, Met staining on the plasma membrane. (F) Cells were treated with BFA (3 µg/ml) for 90 or 180 min, and membranes were immunoblotted for the indicated proteins. p-, phosphorylated protein. Arrow: p170 Met precursor (B,C,F).

Journal of Cell Science (2016) 129, 4238-4251 doi:10.1242/jcs.191684

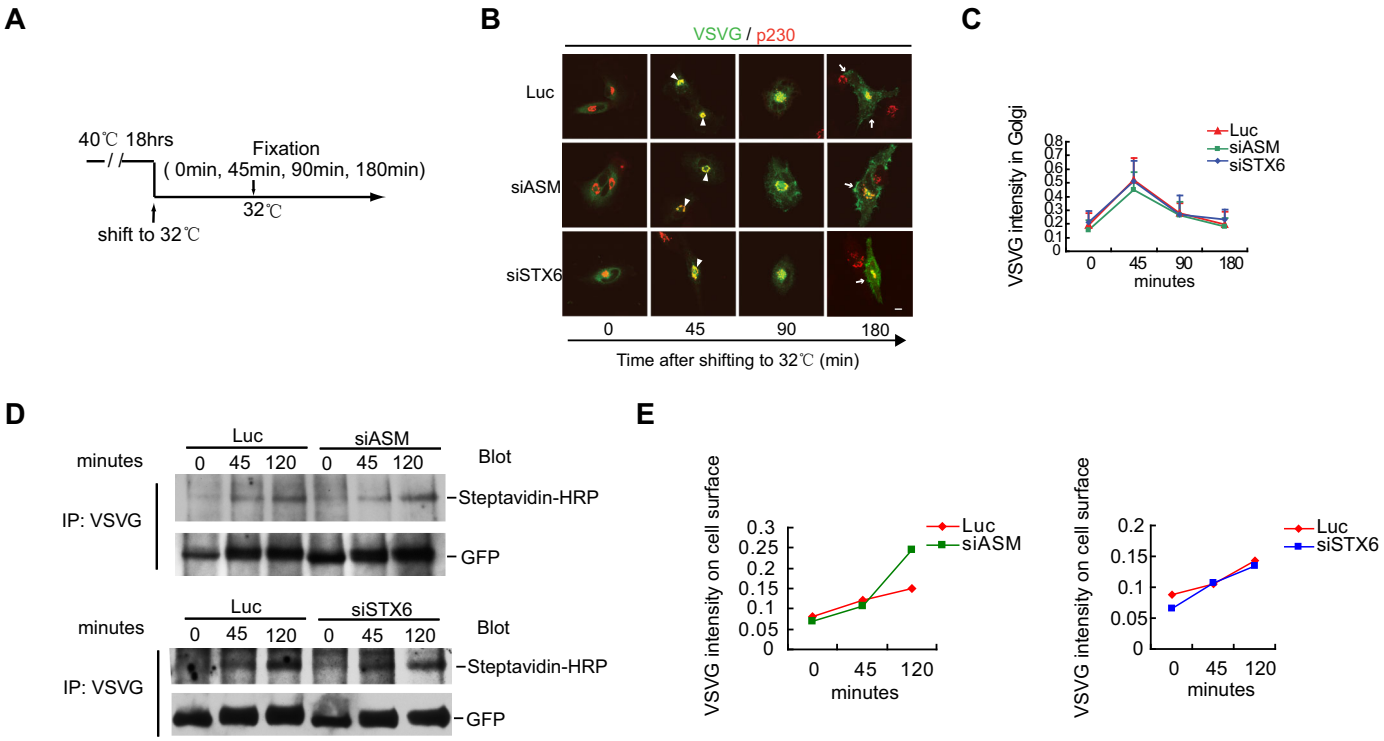

Fig. 5. ASM and STX6 are not required for the Golgi transport of VSVG. (A) An illustration depicting the time course for analyzing the transport of the VSVG-ts045–GFP reporter from the Golgi to the plasma membrane. (B) U373-MG cells, transfected with the reporter plasmid, were cultured at non-permissive temperature 40°C for 18 h. Cells were subsequently shifted to permissive temperature 32°C (time 0), VSVG was detected later in the TGN at 45 min, and then on the plasma membrane at 90 and 180 min in control siRNA (Luc) or in cells transfected with siRNAs against ASM (siASM) and STX6 (siSTX6). Scale bars: 10 µm. Arrowheads, VSVG staining in the Golgi region; arrows, VSVG staining on the plasma membrane. (C) Quantification of the mean of VSVG intensity in the Golgi region (marked by p230) relative to the whole-cell intensity for cells in panel B was performed as described in Fig. 3C. For each condition, at least 50 cells from three independent experiments were analyzed (error bars indicate s.d.). (D,E) U373-MG cells stably expressing the VSVG-ts045–GFP protein were transfected with siASM or siSTX6 for 48 h. After incubation at 40°C for 18 h, cells were shifted to 32°C for the indicated times. Cell surface proteins were biotinylated, cells were lysed and VSVG-ts045–GFP proteins were immunoprecipitated (IP) with anti-VSVG antibodies and analyzed by using SDS-PAGE. The cell-surface-biotinylated VSVG was detected with streptavidin–HRP, and total VSVG was detected with an anti-GFP antibody (D). The relative cell surface VSVG as a percentage of the total VSVG was calculated (E).

analyzed by performing FACS (Fig. S3E). STX6 deficiency also caused an enhanced colocalization of Met with the lysosomal marker LAMP2 (Fig. 6C), similar to that of ASM inactivation (Fig. 3E), and such colocalization was also more pronounced at 72 h as compared with that at 24 h (Fig. S2A). When cells were treated with bafilomycin A1 to inhibit lysosomal protease function, enhanced accumulation of Met was observed in the lysosomes, as revealed by the increased colocalization of Met with the lysosomal marker LAMP2, and quantification in 70 cells further supported this notion (Fig. 6E). Similar results were obtained upon co-staining Met with other lysosomal markers, such as CD63 (Fig. 6F) and LAMP1 (Fig. S2B,C). When the LysoTracker dye was used, colocalization of Met and lysosomes was also confirmed, although in the bafilomycin-A1-treated cells, LysoTracker dye failed to accumulate in the lysosomes owing to the defective vacuolar-type H^+-ATPase function (Fig. S2E,F). In addition, silencing of STX6 also potently suppressed the steady-state levels of Met that was phosphorylated at tyrosine residues, the phosphorylation levels of S6K and, to a lesser degree, the phosphorylation levels of AKT (Fig. 6D). A slight reduction of total Met proteins was also noticed in the STX6-knockdown cells (Fig. 6D, 72 h). Our studies thus showed that knockdown of either ASM or STX6 had similar effects on Met, indicating that ASM and STX6 are likely to function in the same pathway to regulate the trafficking of Met from Golgi to the plasma membrane.

Cholesterol is required for the Golgi exit and plasma membrane delivery of Met

Ceramide, produced through the ASM-mediated hydrolysis of sphingomyelin, has been postulated to work with cholesterol to form a unique type of lipid raft in the plasma membrane (Rajendran and Simons, 2005; van Blitterswijk et al., 2003). Recent studies have shown that the Golgi-associated cholesterol is required for STX6 localization in the TGN and for an STX6-dependent integrin recycling process (Reverter et al., 2014). We tested whether the transport of Met from the Golgi to the plasma membrane is also regulated by cholesterol by treating cells with an oxidized cholesterol analog, 7-ketocholesterol. 7-ketocholesterol has been used to block T-cell receptor signaling by disrupting the cholesterol-dependent lipid rafts (Rentero et al., 2008). We found that U373-MG cells were extremely sensitive to 7-ketocholesterol, and even 15 min of exposure to 7-ketocholesterol affected Met trafficking (Fig. 7). Although Met was largely unaffected when the medium was supplemented with 30 µM cholesterol, treatment of cells with the 7-ketocholesterol:cholesterol mixtures (at 1:2 or 2:1 ratios, total 30 µM) markedly reduced the levels of plasma-membrane-associated Met and caused a dramatic accumulation of Met in the discretely and densely stained TGN area, and those sites of accumulation colocalized with STX6 and p230 (Fig. 7A). Comparison of the linescan intensity profiles further indicated the effects of 7-ketocholesterol on the

Journal of Cell Science (2016) 129, 4238-4251 doi:10.1242/jcs.191684

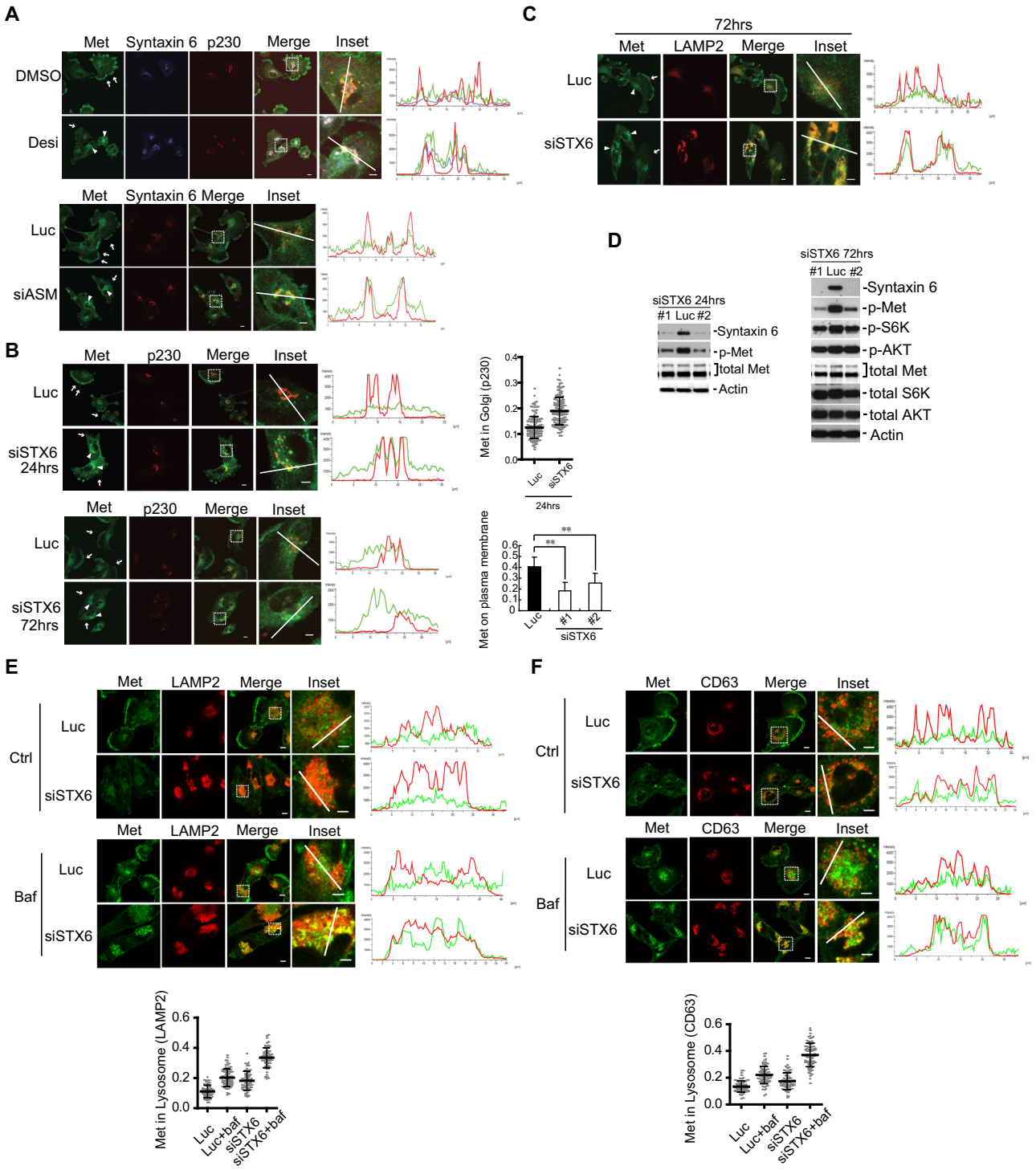

Fig. 6. STX6 regulates Met exit from TGN. (A) U373-MG cells were treated with DMSO or 35 µM desipramine (Desi) for 3 h or transfected with siRNAs against luciferase (Luc) or ASM (#1, siASM) for 24 h, and then co-immunostained for Met (green), STX6 (blue) and p230 (red) as indicated. Insets: enlarged boxed regions. Linescan intensity profiles of Met, STX6 and p230 signals along the white axis lines in insets show strong colocalization and overlap of Met (green), STX6 (blue) and p230 (red) signals in the ASM-inactivated cells, as compared to their weak overlap in the control cells. (B,C) Cells were transfected with siRNAs against luciferase (Luc) or STX6 (#1, siSTX6) for either 24 or 72 h and then co-stained with antibodies against Met and p230 (B) or with antibodies against Met and lysosomal marker LAMP2 (C). In the right-hand panels of B, quantification of the relative Met staining intensity in the Golgi region (marked by p230 staining, top panel) and the plasma-membrane-associated Met (bottom panel) from 100 cells for each indicated condition was conducted as described in Fig. 3C and Fig. 2C, respectively (error bars, s.d.; $^{**}P<0.01$, Student's *t*-test). Arrows, Met staining on the plasma membrane; arrowheads, Met staining in the intracellular compartments (p230- or LAMP2-positive compartments). (D) Cells were treated with siRNA against Luciferase (Luc, control) or STX6 (oligonucleotide #1 or #2). Proteins in the cell lysates were analyzed by immunoblotting for the indicated proteins. p-, phosphorylated protein. (E,F) Cells were treated with control siRNA or siRNA against STX6 (oligonucleotide #1) for 52 h and then treated with or without bafilomycin A1 (Baf, 100 nM) for additional 7 h. Cells were fixed and co-stained for Met and LAMP2 (E) or for Met and CD63 (F) with antibodies, and the relative Met staining in the lysosome region (marked by LAMP2 or CD63 staining, respectively) was quantified from 70 cells for each condition, conducted as described in Fig. 3F and G. Scale bars: 10 µm (all images excluding insets); 5 µm (insets).

Journal of Cell Science (2016) 129, 4238-4251 doi:10.1242/jcs.191684

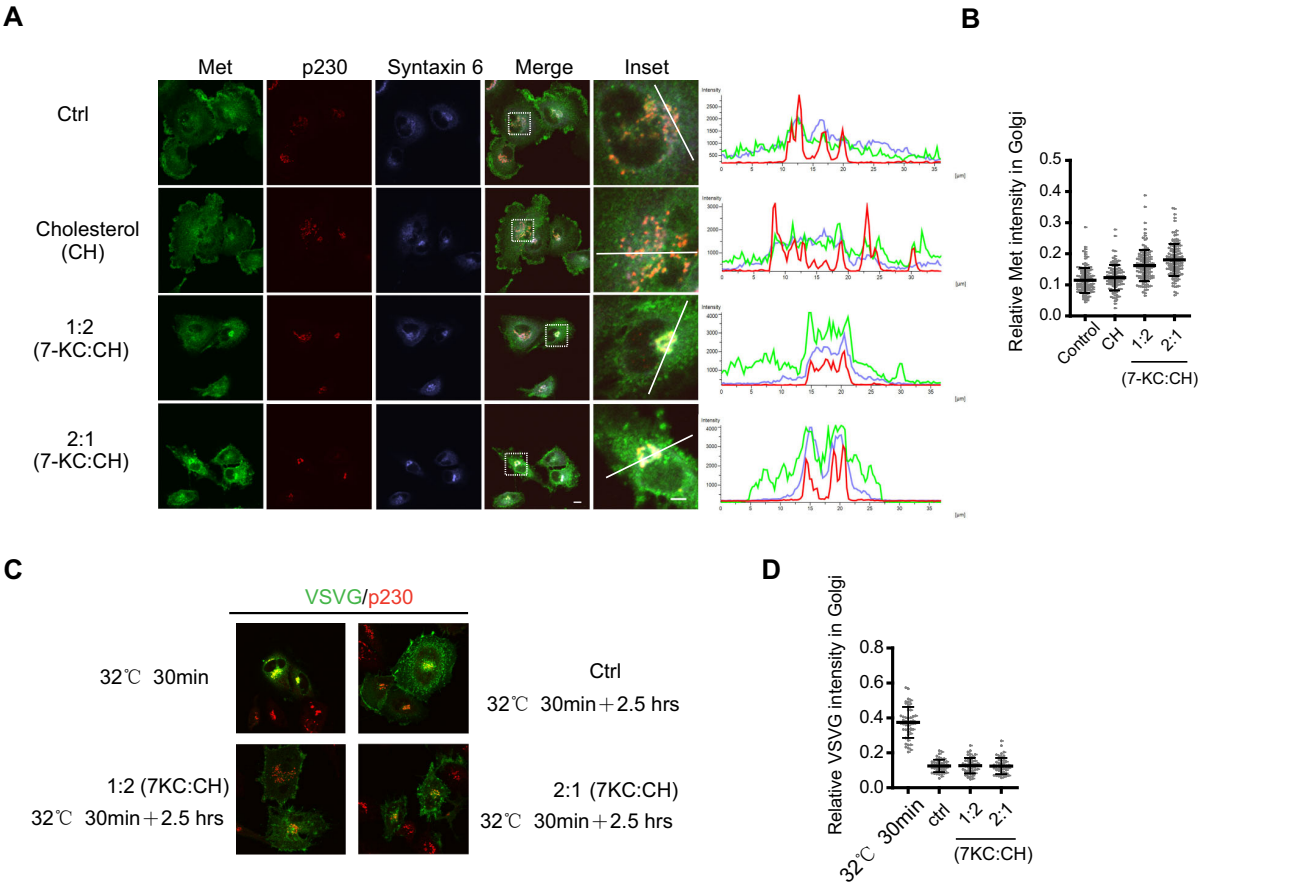

Fig. 7. Cholesterol depletion blocks Met in the TGN. (A) U373-MG cells were treated for 15 min either with vehicle, cholesterol (30 µM), a mixture of 7-ketocholesterol (7-KC) and cholesterol (CH) at a 1:2 ratio (10 µM 7-KC:20 µM CH) or at 2:1 ratio (20 µM 7-KC:10 µM CH) as indicated. Cells were co-immunostained for Met, STX6 and p230. Insets: enlarged boxed regions. Fluorescence intensity profiles of Met, STX6 and p230 staining signals along the white lines show enhanced colocalization of these proteins in response to 7-ketocholesterol. Scale bar: 10 µm (all images except insets); 5 µm (inset images). (B) Quantification of the relative Met staining intensity in the Golgi region (marked by p230 staining) from 100 cells under each condition; conducted as described in Fig. 3C. (C) U373-MG cells stably expressing the VSVG-ts045–GFP protein were incubated at 40°C for 18 h and shifted to 32°C for 30 min, which served as the starting point (top left). Cells were treated with or without 7-KC and incubated at 32°C for another 2.5 h, fixed and stained for p230 (red) with antibodies, and VSVG-ts045–GFP was detected by GFP green fluorescence. (D) Quantification of the mean of VSVG intensities in the Golgi region (marked by p230) relative to the whole-cell intensity for 50 cells under each indicated condition was performed as described in Fig. 5C, and data are plotted as a scatter plot.

colocalization of Met, STX6 and p230 (Fig. 7A). Quantification of the Golgi-localized Met from 100 cells for each condition (from three experiments) also clearly showed the effects of 7-ketocholesterol (Fig. 7B). These observations suggest that cholesterol is required for the Golgi exit of Met.

We also examined if cholesterol depletion affects the Golgi exit of VSVG in our cells. Using the system described in Fig. 5, we found that at the concentration of 7-ketocholesterol that inhibits Met exit from Golgi, the exit of VSVG–GFP from the Golgi was not inhibited by cholesterol depletion, as revealed by the similar kinetics of clearance of Golgi-localized VSVG-ts045–GFP (Fig. 7C, and quantified in Fig. 7D). These observations suggest that cholesterol is not required for the Golgi exit of VSVG.

ASM and STX6 are required for the ligand-dependent activation of Met

Our data so far have shown that knockdown of ASM or STX6 each reduced the levels of the tyrosine-phosphorylated and activated Met in the asynchronously growing U373-MG cells. To determine if the pool of Met generated from the biosynthetic ER–Golgi process actively participates in the signaling response induced by HGF, we examined whether the ligand-induced activation of Met is affected by ASM or STX6 inactivation. We first treated cells with desipramine or siRNAs against ASM or STX6, or with controls, and the cells were further serum-starved and then stimulated with HGF. In control cells, HGF stimulation led to a rapid induction of Met phosphorylation at Y1234 and Y1235 and of S6K phosphorylation; however, such phosphorylation events were substantially attenuated in the ASM- or STX6-inactivated cells (Fig. 8A–C). Brief treatment with BFA also produced a similar inhibitory effect (Fig. 8D). The sensitivity of the HGF-dependent Met activation to BFA suggests that the maintenance of Met levels on the plasma membrane requires the continued replenishment with the biosynthesized Met coming from the Golgi.

To further determine the involvement of ASM in regulation of Met signaling, we examined the HGF-induced Met tyrosine phosphorylation and actin cytoskeleton reorganization in individual cells by immunostaining. HGF treatment induced a strong appearance of the Y1234- and Y1235-phosphorylated Met on the plasma membrane, which was absent in the unstimulated cells and also prevented by the desipramine pre-treatment (Fig. 8E). Similarly, knockdown of ASM by siRNAs also effectively reduced the levels of HGF-induced tyrosine-phosphorylated Met at the plasma membrane (Fig. 8E). We further asked whether the

Journal of Cell Science (2016) 129, 4238-4251 doi:10.1242/jcs.191684

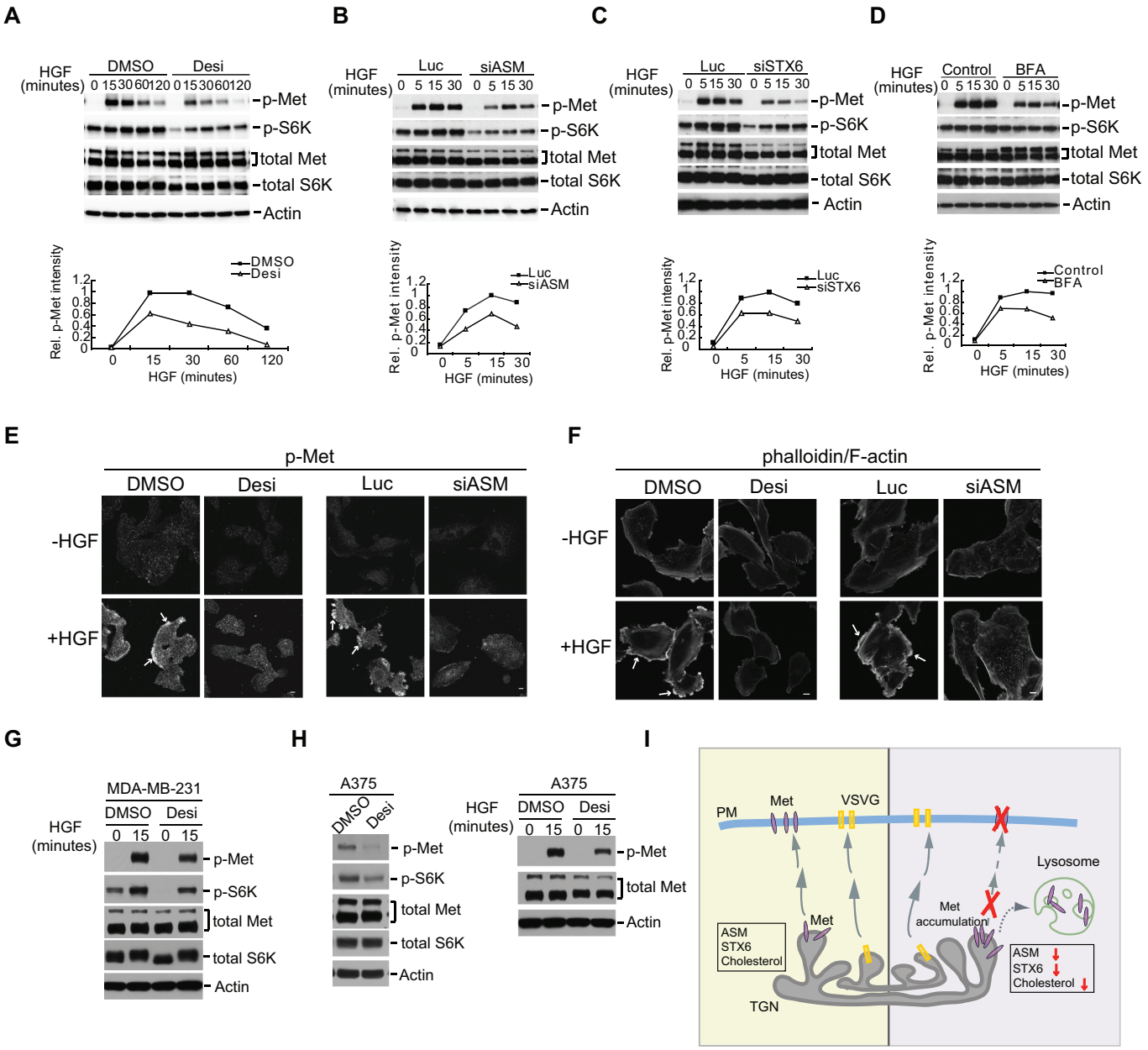

Fig. 8. Inactivation of ASM or STX6 blocks the ligand-induced Met activation and downstream signaling. (A) U373-MG cells were treated with DMSO or 30 µM desipramine (Desi) for 18 h. The cells were further serum-starved with or without 30 µM desipramine for 3 h and then stimulated with HGF (50 ng/ml) for the indicated times. (B,C) Similar to A, except that cells were transfected with control siRNA (Luc) or siRNAs against ASM (B, siASM) or STX6 (C, siSTX6) and then then starved and re-stimulated with HGF. (D) Similar to A, except cells were treated with 3 µg/ml BFA during serum starvation for 3 h before HGF re-stimulation. In A–D, proteins were detected using the indicated antibodies and the relative (Rel.) band intensities of phosphorylated Met (p-Met) to that of the total Met proteins were quantified using actin as a loading control. Control, without drug addition. (E,F) U373-MG cells were treated with desipramine or siRNAs against ASM as in A and B. The cells were serum-starved and then stimulated with HGF for 15 min. Cells were immunostained with an antibody detecting Y1234- and Y1235-phosphorylated Met (p-Met) (E) or with phalloidin for F-actin (F). Arrows in E, p-Met staining on the plasma membrane; arrows in F, F-actin staining. Scale bars: 10 µm. (G,H) Breast cancer MDA-MB-231 cells (G) or melanoma A375 cells (H, right panels) were treated with DMSO or 30 µM desipramine for 18 h. The cells were serum-starved with or without 30 µM desipramine for 3 h and then stimulated with HGF (50 ng/ml) for 15 min as indicated. A375 cells were also treated with DMSO or 30 µM desipramine for 18 h in regular growth medium without starvation and HGF treatment (H, left panels). The levels of phosphorylated Met (p-Met) and phosphorylated S6K (p-S6K), as well as the total levels of Met and S6K were analyzed. For total Met, the upper band represents the p170 form, and the lower band represents the p145 form. (I) A model for ASM or STX6 function on the regulation of Met protein traffic. ASM, STX6 and cholesterol regulate a unique subdomain on the TGN that is required for Met protein transport, whereas a different subdomain on the TGN is used for VSVG protein transport. Prolonged trapping of Met in the TGN after loss of ASM or STX6 subsequently induces aberrant trafficking of Met to lysosomes and then degradation of Met. PM, plasma membrane.

HGF-induced cytoskeleton changes, monitored by staining with phalloidin – a toxin that strongly binds to F-actin – were sensitive to ASM inhibition. Indeed, HGF induced a strong cytoskeleton actin reorganization response in control cells, and such a response was absent in cells that had been pre-treated with desipramine or siRNAs against ASM (Fig. 8F). These studies again demonstrate that ASM is required for the HGF-induced Met activation and its downstream signaling to regulate cytoskeleton reorganization.

Journal of Cell Science (2016) 129, 4238-4251 doi:10.1242/jcs.191684

ASM regulates the levels of phosphorylated Met in breast cancer and melanoma cells

Our analysis of ASM expression profiles also revealed that ASM is highly expressed in melanoma and breast cancer cells (Fig. S1A). To test whether ASM also regulates Met in cancer cells other than GBM cells, we examined the response of activated Met in the breast cancer cell line MDA-MB-231 and melanoma cell line A375 to ASM inhibition, and these cells have been reported to have increased Met expression and activation (Cao et al., 2015; Hochgrafe et al., 2010). We found that treatment with desipramine reduced the HGF-induced levels of the phosphorylated Met protein in both cancer cell lines (Fig. 8G,H) and in the actively growing A375 cells (Fig. 8H). Similar to in GBM cells, inhibition of ASM also caused decreased levels of the phosphorylated S6 kinase (Fig. 8G,H). These studies indicate that ASM regulates the activation state of cell-surface-localized Met in various cancer cells.

DISCUSSION

In this report, we found that ASM regulates the cell surface levels of Met. Our studies revealed that ASM controls the levels of tyrosine-phosphorylated and activated Met in both actively growing cells and in ligand-stimulated cells. Our results demonstrate that the level of the Met protein on the plasma membrane is dynamically replenished by its intracellular pools. One pathway is through the anterograde transport from the TGN, which supplies the biosynthesized Met protein to the plasma membrane. We showed that this pathway is dependent on ASM, STX6 and cholesterol. In comparison, the Golgi exit of VSVG, a non-RTK protein, is independent of ASM, STX6 and cholesterol. Our results are summarized in a model in which distinct subdomains on the TGN are used for the exit of different cargos from the Golgi (Fig. 8I). We propose that the ASM activity is required for the exit of Met proteins from the TGN for delivery to the plasma membrane. Reduced levels of ASM or STX6 selectively blocked Met from exit of this subdomain of the TGN. In the absence of either ASM or STX6, Golgi-trapped Met proteins aberrantly trafficked to the lysosome, promoting their proteolytic degradation in this organelle. As ASM and STX6 inactivation both trap Met in TGN, it is possible that ASM and STX6 either act in a linear pathway or act in parallel pathways to regulate the exit of Met from the Golgi. Our data further show that ASM regulates STX6 localization; therefore, it supports the possibility of a linear pathway, with STX6 being a downstream effector of ASM in the process. In addition, we found that this exit process also requires the participation of cholesterol. The subdomain of the TGN used for the transport of Met proteins is distinct from that of the TGN used for VSVG exit (Fig. 8I). Notably, STX6 has been implicated in regulating the Golgi exit of VEGFR in endothelial cells (Manickam et al., 2011).

Although the Golgi exit transport system is mostly thought to be a constitutive process, our new findings on the regulation of Met protein transport by ASM provide strong evidence that the Golgi exit of certain cargos is a highly selective process that is regulated by ASM, STX6 and cholesterol. How does ASM contribute to this process? One possibility is that ASM-mediated conversion of sphingomyelin to ceramide regulates the lipid composition of the plasma membrane as well as the membranes of endosomes and Golgi, owing to the rapid equilibrium between these membrane systems. Consequently, loss of ASM could alter the Golgi membrane lipid composition, leading to a failure of exit of the Met protein from the TGN. Recent studies have suggested that sphingomyelin might be involved in forming lipid rafts in the Golgi membranes (Duran et al., 2012), although the involvement of ceramides has not been established. It has been shown that inhibition of Golgi sphingomyelin synthesis through knocking down the gene encoding sphingomyelin synthase 1 (*SMS1*) or forced formation of short chain sphingomyelins at the Golgi through incorporation of a short-chain ceramide analog leads to a defect in the general transport function of the Golgi, as measured using the VSVG cargo (Duran et al., 2012; Subathra et al., 2011). In comparison, our studies showed that inactivation of ASM caused a defect in the selective transport of Met at the Golgi, but not in that of VSVG. Our studies suggest a new level of regulation of the TGN function through ASM-dependent sphingomyelin hydrolysis and ceramide production. We have also observed that ASM inactivation greatly reduces the appearance of Met proteins in the lamellipodia regions on the cell surface (Figs 2 and 3). Knockdown of STX6 and loss of cholesterol had similar effects on this RTK (Figs 6 and 7). These observations raise the possibility that ASM, STX6 and cholesterol are involved in the regulation of the delivery of a selective set of cargos to the lamellipodia, which is often the leading edge for cell migration. Our studies are consistent with recent reports that suggest the importance of the TGN in establishing cell polarity through controlling polarized intracellular transport (Zhu and Kaverina, 2013). Furthermore, given the fact that the Met RTK is frequently overexpressed in GBMs, melanoma and breast cancers, combined with our finding that ASM is highly expressed in these cancers (Fig. S1A), our results suggest that deregulation of ASM could contribute to the aberrant Met expression and activation found in these cancers. As we have demonstrated that inactivation of ASM can effectively reduce both the Met receptor levels and their downstream signaling, our studies also suggest that ASM might serve as a novel therapeutic target for GBM and other cancers, including melanoma and breast cancers, that overexpress Met and ASM.

MATERIALS AND METHODS

Cells, antibodies and immunofluorescence

Human GBM U373-MG, U251-MG, U87-MG, LN18, U118-MG, breast cancer MDA-MB-231 and melanoma A375 cells were obtained from American Type Culture Collection (ATCC). Recombinant human HGF and Alexa-Fluor-568–phalloidin were purchased from Life Technologies. Antibodies against ASM (mouse), Met (goat or mouse, APC conjugate) STX6 (sheep, biotin conjugate), and control IgG (mouse, APC conjugate) were from R&D Systems. Rabbit antibodies against Met, phosphorylated Met (at Y1234 and Y1235), phosphorylated S6K (at T389), phosphorylated AKT (at S473, recognizing all AKT isoforms), S6K, AKT (recognizing all isoforms), STX6 and IGF1R were from Cell Signaling. Monoclonal antibodies against integrin β3, LAMP1, CD63, p230, GM130 and STX6 were from BD Biosciences. Anti-VSVG and anti-GFP antibodies were from Bethyl and Santa Cruz Biotechnology, respectively. Alexa-Fluor-488-conjugated goat anti-mouse IgG, Alexa-Fluor-488-conjugated anti-rabbit IgG, Alexa-Fluor-647-conjugated anti-mouse IgG and Alexa-Fluor-647-conjugated anti-rabbit IgG antibodies were from Jackson Immunologicals. Brilliant-Violet-421-conjugated Streptavidin was from BioLegend. Streptavidin–HRP, sulfo-NHS-LC-biotin and bafilomycin A1 were from Pierce (Thermo), Thermo Scientific and LC Laboratories, respectively. Immunoprecipitation and western blotting analyses were conducted as described previously (Zhang et al., 2013), and quantification of protein band intensity was performed using the Fiji (Image J) software (Schindelin et al., 2012). See Table S1 for further details.

Plasmids and siRNAs

The temperature-sensitive mutant VSVG-ts045–GFP was obtained from Addgene. The siRNA duplexes (Dharmacon) used were: Met #1: GAGAC-AUCAUAGUGCUAGU, #2: UGCCAAAAUUGCACUAUUA; IGF1R #1: GACCAUCAAAGCAGGGAAA, #2: UUACCGGAAAGGAGGGAAA; ASM #1: UGGCCAUCAAGCUGUGCAA, #2: CUGCCCAAUCUGCA-AAGGU; STX6 #1: AGAGCCAAUUCUCAUUUCA, #2: GAUGAAGA

AACUUGCAAAA; and Luciferase (CGUACGCGGAAUACUUCGA). All sequences are given 5′ to 3′. Transfection of siRNAs (50 nM) or plasmids (1 µg) was conducted using Oligofectamine (Life Technologies) or FuGene 6 (Promega), as described previously (Zhang et al., 2013).

Immunofluorescence imaging and flow cytometry

Cells were fixed and permeabilized with Fixation and Permeabilization Solution (BD Biosciences), blocked with goat serum, incubated with primary antibodies and then secondary antibodies, and counterstained with 4′, 6-Diamidine-2′-phenylindole dihydrochloride (DAPI). Images were acquired using the 40×1.3 numerical aperture (NA) oil immersion objective lens with settings kept constant for each set of experiments with a Nikon A1R confocal laser scanning microscopy system equipped with the NIS-Elements Advance Research software. The captured images were further analyzed and quantified by using the Fiji (ImageJ) software (Schindelin et al., 2012). For flow cytometry analyses, cells were detached using Accutase Cell Detachment Solution (BD Biosciences) and then incubated with monoclonal antibodies against Met or with mouse IgG control antibody (APC conjugated) for 40 min at 4°C. Cells were washed, and cell surface fluorescence was measured using the BD FACSCalibur Flow Cytometry instrument.

^{35}S-labeling of proteins

Cells were labeled with 0.5 mCi/dish of ^{35}S-labeled methionine and ^{35}S-labeled cysteine, obtained from Perkin Elmer (NEG072014, 11 mCi/ml, 14 mCi total, >1000 Ci/mmol), for various times in cell culture medium that lacked methionine and cysteine and that was supplemented with 10% dialyzed FBS. The cells were processed for immunoprecipitation, and analyzed by using gel electrophoresis and fluorography, as described previously (Zhang et al., 1995).

Cell surface biotinylation

Biotinylation of cell surface proteins was performed as described previously (Roberts et al., 2001) by incubating cells at 4°C for 30 min in phosphate-buffered-saline (PBS) containing freshly prepared sulfo-NHS-LC-biotin (0.5 mg/ml). Unreacted biotin was blocked with 100 mM glycine in PBS. Cells were washed and then lysed in the NP40-containing lysis buffer and processed for anti-Met or anti-VSVG immunoprecipitation, and biotinylated proteins were detected by using HRP-conjugated streptavidin.

7-ketocholesterol and cholesterol assay

50 mg/ml methyl-β-cyclodextrin (mβCD) complexed to 1.5 mg/ml 7-ketocholesterol was prepared as described previously (Rentero et al., 2008). Briefly, 4×10-µl aliquots of 15 mg/ml 7-ketocholesterol in ethanol were added to 360 µl of 50 mg/ml mβCD every 5–10 min. Cells were incubated with 7.5 µl in total of stock solutions of mβCD-cholesterol, mβCD–7-ketocholesterol or a combination of the two sterols diluted in 1 ml Dulbecco's modified Eagle's medium (containing 1% FBS, 0.5 mg/ml BSA) for the indicated times before cells were fixed and processed for immunostaining.

Statistics and bioinformatics

Quantitative data are expressed as the mean±s.d., and plots were prepared using the GraphPad Prism 5 software. Statistically significant differences between means were determined using a two-tailed equal-variance Student's *t*-test (Fay and Gerow, 2013). Different data sets were considered to be statistically significant when the *P*-value was <0.05 (*), 0.01 (**) or 0.001 (***).

Acknowledgements

Confocal imaging was performed at the University of Nevada, Las Vegas Confocal and Biological Imaging Core, with assistance of Sophie Choe.

Competing interests

The authors declare no competing or financial interests.

Author contributions

H.S. conceived the idea and analyzed the data, L.Z. organized and conducted most of the experiments, with assistance from X.X., Y.K., N.O and F.L. H.S. and H.Z. wrote the manuscript.

Funding

This work was supported by grants from U.S. Department of Defense (W81XWH-09-1-0551 to H.S.), National Institutes of Health (R15GM116087 to H.Z.) and National Natural Science Foundation of China (NSFC21133002 to H.Z.). Deposited in PMC for release after 12 months.

Supplementary information

Supplementary information available online at
http://jcs.biologists.org/lookup/doi/10.1242/jcs.191684.supplemental

References

Akasaki, K., Michihara, A., Fujiwara, Y., Mibuka, K. and Tsuji, H. (1996). Biosynthetic transport of a major lysosome-associated membrane glycoprotein 2, lamp-2: a significant fraction of newly synthesized lamp-2 is delivered to lysosomes by way of early endosomes. *J. Biochem.* **120**, 1088-1094.

Cao, H.-H., Cheng, C.-Y., Su, T., Fu, X.-Q., Guo, H., Li, T., Tse, A. K.-W., Kwan, H.-Y., Yu, H. and Yu, Z.-L. (2015). Quercetin inhibits HGF/c-Met signaling and HGF-stimulated melanoma cell migration and invasion. *Mol. Cancer* **14**, 103.

Choudhury, A., Marks, D. L., Proctor, K. M., Gould, G. W. and Pagano, R. E. (2006). Regulation of caveolar endocytosis by syntaxin 6-dependent delivery of membrane components to the cell surface. *Nat. Cell Biol.* **8**, 317-328.

Clague, M. J. (2011). Met receptor: a moving target. *Sci. Signal.* **4**, pe40.

Cremesti, A., Paris, F., Grassme, H., Holler, N., Tschopp, J., Fuks, Z., Gulbins, E. and Kolesnick, R. (2001). Ceramide enables fas to cap and kill. *J. Biol. Chem.* **276**, 23954-23961.

Duran, J. M., Campelo, F., van Galen, J., Sachsenheimer, T., Sot, J., Egorov, M. V., Rentero, C., Enrich, C., Polishchuk, R. S., Goñi, F. M. et al. (2012). Sphingomyelin organization is required for vesicle biogenesis at the Golgi complex. *EMBO J.* **31**, 4535-4546.

Engelman, J. A., Zejnullahu, K., Mitsudomi, T., Song, Y., Hyland, C., Park, J. O., Lindeman, N., Gale, C.-M., Zhao, X., Christensen, J. et al. (2007). MET amplification leads to gefitinib resistance in lung cancer by activating ERBB3 signaling. *Science* **316**, 1039-1043.

Fay, D. S. and Gerow, K. (2013). A biologist's guide to statistical thinking and analysis. *WormBook* 1-54.

Gleeson, P. A., Lock, J. G., Luke, M. R. and Stow, J. L. (2004). Domains of the TGN: coats, tethers and G proteins. *Traffic* **5**, 315-326.

Grassmé, H., Jekle, A., Riehle, A., Schwarz, H., Berger, J., Sandhoff, K., Kolesnick, R. and Gulbins, E. (2001). CD95 signaling via ceramide-rich membrane rafts. *J. Biol. Chem.* **276**, 20589-20596.

Hirschberg, K., Miller, C. M., Ellenberg, J., Presley, J. F., Siggia, E. D., Phair, R. D. and Lippincott-Schwartz, J. (1998). Kinetic analysis of secretory protein traffic and characterization of golgi to plasma membrane transport intermediates in living cells. *J. Cell Biol.* **143**, 1485-1503.

Hochgrafe, F., Zhang, L., O'Toole, S. A., Browne, B. C., Pinese, M., Porta Cubas, A., Lehrbach, G. M., Croucher, D. R., Rickwood, D., Boulghourjian, A. et al. (2010). Tyrosine phosphorylation profiling reveals the signaling network characteristics of Basal breast cancer cells. *Cancer Res.* **70**, 9391-9401.

Jaffrézou, J.-P., Chen, G., Durán, G. E., Muller, C., Bordier, C., Laurent, G., Sikic, B. I. and Levade, T. (1995). Inhibition of lysosomal acid sphingomyelinase by agents which reverse multidrug resistance. *Biochim. Biophys. Acta* **1266**, 1-8.

Jeffers, M., Taylor, G. A., Weidner, K. M., Omura, S. and Vande Woude, G. F. (1997). Degradation of the Met tyrosine kinase receptor by the ubiquitin-proteasome pathway. *Mol. Cell. Biol.* **17**, 799-808.

Jenkins, R. W., Canals, D. and Hannun, Y. A. (2009). Roles and regulation of secretory and lysosomal acid sphingomyelinase. *Cell. Signal.* **21**, 836-846.

Jenkins, R. W., Idkowiak-Baldys, J., Simbari, F., Canals, D., Roddy, P., Riner, C. D., Clarke, C. J. and Hannun, Y. A. (2011). A novel mechanism of lysosomal acid sphingomyelinase maturation: requirement for carboxyl-terminal proteolytic processing. *J. Biol. Chem.* **286**, 3777-3788.

Joffre, C., Barrow, R., Ménard, L., Calleja, V., Hart, I. R. and Kermorgant, S. (2011). A direct role for Met endocytosis in tumorigenesis. *Nat. Cell Biol.* **13**, 827-837.

Kim, Y. and Sun, H. (2007). Functional genomic approach to identify novel genes involved in the regulation of oxidative stress resistance and animal lifespan. *Aging Cell* **6**, 489-503.

Kim, Y. and Sun, H. (2012). ASM-3 acid sphingomyelinase functions as a positive regulator of the DAF-2/AGE-1 signaling pathway and serves as a novel anti-aging target. *PLoS ONE* **7**, e45890.

Klausner, R. D., Donaldson, J. G. and Lippincott-Schwartz, J. (1992). Brefeldin A: insights into the control of membrane traffic and organelle structure. *J. Cell Biol.* **116**, 1071-1080.

Komada, M., Hatsuzawa, K., Shibamoto, S., Ito, F., Nakayama, K. and Kitamura, N. (1993). Proteolytic processing of the hepatocyte growth factor/scatter factor receptor by furin. *FEBS Lett.* **328**, 25-29.

Koochekpour, S., Jeffers, M., Rulong, S., Taylor, G., Klineberg, E., Hudson, E. A., Resau, J. H. and Vande Woude, G. F. (1997). Met and hepatocyte growth factor/scatter factor expression in human gliomas. *Cancer Res.* **57**, 5391-5398.

Lin, L. and Bivona, T. G. (2012). Mechanisms of resistance to epidermal growth factor receptor inhibitors and novel therapeutic strategies to overcome resistance in NSCLC patients. *Chemother. Res. Pract.* **2012**, 817297.
Lingwood, D. and Simons, K. (2010). Lipid rafts as a membrane-organizing principle. *Science* **327**, 46-50.
Lippincott-Schwartz, J., Yuan, L., Tipper, C., Amherdt, M., Orci, L. and Klausner, R. D. (1991). Brefeldin A's effects on endosomes, lysosomes, and the TGN suggest a general mechanism for regulating organelle structure and membrane traffic. *Cell* **67**, 601-616.
Maher, E. A., Furnari, F. B., Bachoo, R. M., Rowitch, D. H., Louis, D. N., Cavenee, W. K. and DePinho, R. A. (2001). Malignant glioma: genetics and biology of a grave matter. *Genes Dev.* **15**, 1311-1333.
Manickam, V., Tiwari, A., Jung, J.-J., Bhattacharya, R., Goel, A., Mukhopadhyay, D. and Choudhury, A. (2011). Regulation of vascular endothelial growth factor receptor 2 trafficking and angiogenesis by Golgi localized t-SNARE syntaxin 6. *Blood* **117**, 1425-1435.
Maroun, C. R. and Rowlands, T. (2014). The Met receptor tyrosine kinase: a key player in oncogenesis and drug resistance. *Pharmacol. Ther.* **142**, 316-338.
Miller, S. G., Carnell, L. and Moore, H. H. (1992). Post-Golgi membrane traffic: brefeldin A inhibits export from distal Golgi compartments to the cell surface but not recycling. *J. Cell Biol.* **118**, 267-283.
Presley, J. F., Cole, N. B., Schroer, T. A., Hirschberg, K., Zaal, K. J. and Lippincott-Schwartz, J. (1997). ER-to-Golgi transport visualized in living cells. *Nature* **389**, 81-85.
Rajendran, L. and Simons, K. (2005). Lipid rafts and membrane dynamics. *J. Cell Sci.* **118**, 1099-1102.
Rentero, C., Zech, T., Quinn, C. M., Engelhardt, K., Williamson, D., Grewal, T., Jessup, W., Harder, T. and Gaus, K. (2008). Functional implications of plasma membrane condensation for T cell activation. *PLoS ONE* **3**, e2262.
Reverter, M., Rentero, C., Garcia-Melero, A., Hoque, M., Vilà de Muga, S., Álvarez-Guaita, A., Conway, J. R. W., Wood, P., Cairns, R., Lykopoulou, L. et al. (2014). Cholesterol regulates Syntaxin 6 trafficking at trans-Golgi network endosomal boundaries. *Cell Rep.* **7**, 883-897.
Roberts, M., Barry, S., Woods, A., van der Sluijs, P. and Norman, J. (2001). PDGF-regulated rab4-dependent recycling of alphavbeta3 integrin from early endosomes is necessary for cell adhesion and spreading. *Curr. Biol.* **11**, 1392-1402.
Schindelin, J., Arganda-Carreras, I., Frise, E., Kaynig, V., Longair, M., Pietzsch, T., Preibisch, S., Rueden, C., Saalfeld, S., Schmid, B. et al. (2012). Fiji: an open-source platform for biological-image analysis. *Nat. Methods* **9**, 676-682.
Schuchman, E. H. (2007). The pathogenesis and treatment of acid sphingomyelinase-deficient Niemann-Pick disease. *J. Inherit. Metab. Dis.* **30**, 654-663.
Stommel, J. M., Kimmelman, A. C., Ying, H., Nabioullin, R., Ponugoti, A. H., Wiedemeyer, R., Stegh, A. H., Bradner, J. E., Ligon, K. L., Brennan, C. et al. (2007). Coactivation of receptor tyrosine kinases affects the response of tumor cells to targeted therapies. *Science* **318**, 287-290.
Subathra, M., Qureshi, A. and Luberto, C. (2011). Sphingomyelin synthases regulate protein trafficking and secretion. *PLoS ONE* **6**, e23644.
van Blitterswijk, W. J., van der Luit, A. H., Veldman, R. J., Verheij, M. and Borst, J. (2003). Ceramide: second messenger or modulator of membrane structure and dynamics? *Biochem. J.* **369**, 199-211.
Yoshimori, T., Yamamoto, A., Moriyama, Y., Futai, M. and Tashiro, Y. (1991). Bafilomycin A1, a specific inhibitor of vacuolar-type H(+)-ATPase, inhibits acidification and protein degradation in lysosomes of cultured cells. *J. Biol. Chem.* **266**, 17707-17712.
Zhang, H., Kobayashi, R., Galaktionov, K. and Beach, D. (1995). p19Skp1 and p45Skp2 are essential elements of the cyclin A-CDK2 S phase kinase. *Cell* **82**, 915-925.
Zhang, X., Lu, F., Wang, J., Yin, F., Xu, Z., Qi, D., Wu, X., Cao, Y., Liang, W., Liu, Y. et al. (2013). Pluripotent stem cell protein Sox2 confers sensitivity to LSD1 inhibition in cancer cells. *Cell Rep.* **5**, 445-457.
Zhu, X. and Kaverina, I. (2013). Golgi as an MTOC: making microtubules for its own good. *Histochem. Cell Biol.* **140**, 361-367.

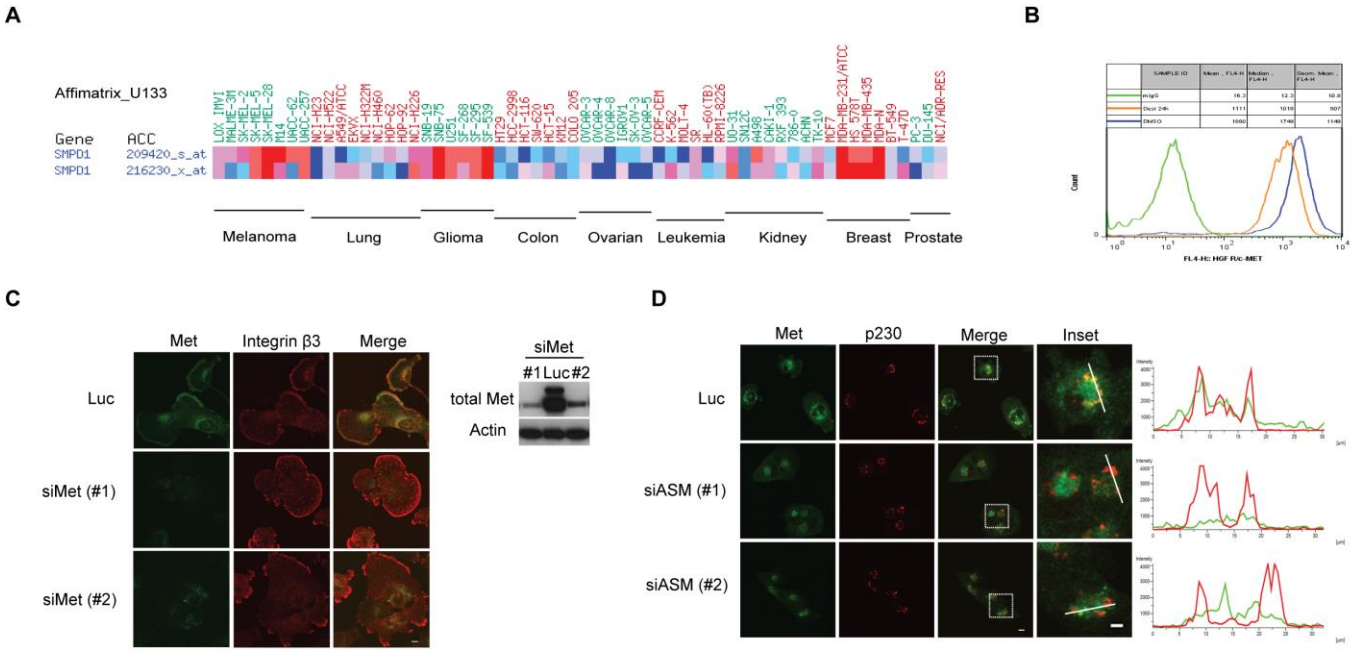

Fig. S1. Expression of ASM in various cancer cells and regulation of Met distribution by ASM. (A) The expression of ASM (SMPD1) in various cancer cell lines was analyzed using the microarray mRNA data of the Cancer Genome Anatomy Project database (https://discover.nci.nih.gov/cellminer/) in 60 cancer cell lines collected by National Cancer Institute. ASM/SMPD1 was highly expressed in several cancer cells including glioma/glioblastoma cells as indicated. (B) Histograms of FACS to detect cell surface Met. U373-MG cells were treated with DMSO and 30 M desipramine as in Fig. 2E. Live cells were detached using the Accutase Cell Detachment Solution and processed for surface staining of live cells with a monoclonal IgG control and an anti-Met monoclonal APC-conjugated antibody (orange and blue fluorescence intensities). Cell surface fluorescence of labeled Met was measured using Flow Cytometry (FACS). Green fluorescence: monoclonal IgG control cells, orange fluorescence: desipramine treated cells, and blue fluorescence: DMSO treated control cells. (C) The immunofluorescence stainings of Met reveal the specific presence of Met on the plasma membrane and intracellular compartments. U373-MG cells were transfected with 50 nM luciferase (control) siRNA and two independent siRNAs against Met. After 48 hours transfection, cells were fixed, stained for Met and integrin 3 as in Fig. 2D, or harvested for examining Met ablation by western blot as indicated. Scale bar, 10 m. (D) Ablation of ASM by siRNAs and desipramine produce the same intracellular trapping of Met in the TGN marked by p230. U373-MG cells were transfected with 50 nM luciferase siRNA and two independent siRNAs against ASM. 72 hours post-transfection, both control and ASM siRNA treated cells were exposed to 35 M desipramine for 2 hours as in Fig. 2A. Cells were fixed and stained with specific antibodies for Met and p230. Scale bar, 10 m. No additive effects of desipramine after siRNA-mediated ASM ablation were found.

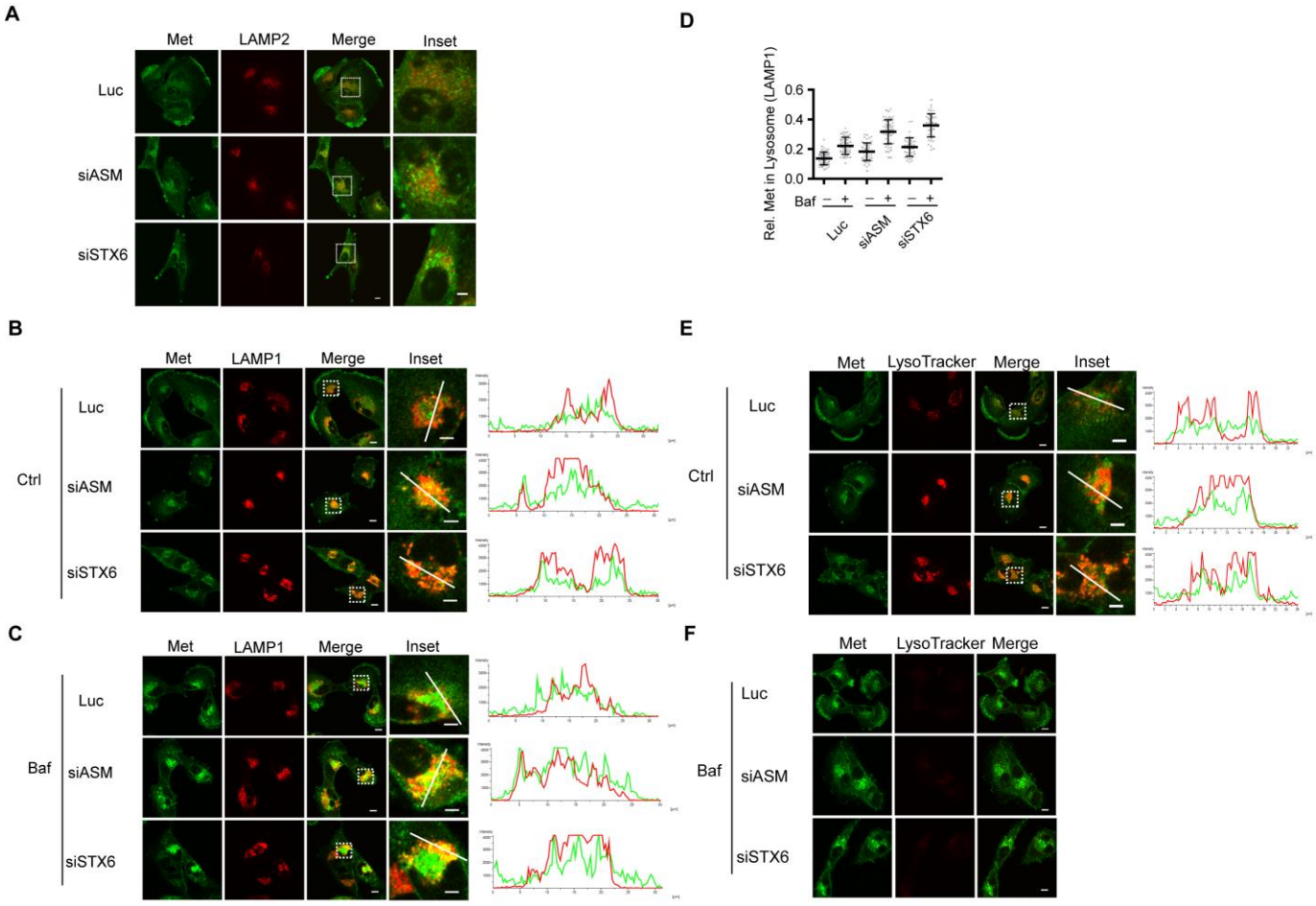

Figure S2. Loss of ASM or STX6 leads to aberrant traffic of Met to lysosomes. (A) U373 cells were transfected with siRNAs against luciferase, ASM, and STX6 for 24 hours, and processed as in Fig. 5F. Cells were fixed and stained with specific antibodies against Met and LAMP2. Scale bar, 10 m. (B-F) Cells were treated with control, ASM or STX6 siRNAs for 52 hours and then treated with bafilomycin A1 (Baf, 100 nM) for additional 7 hours where indicated. Cells were fixed and co-stained with anti-Met and LAMP1 antibodies (B and C) or anti-Met antibody and LysoTracker (E, F), and processed as in Fig. 3. Quantification of relative Met staining in the lysosome region (marked by LAMP1 staining) was carried out as described in Fig. 3F in 3G.

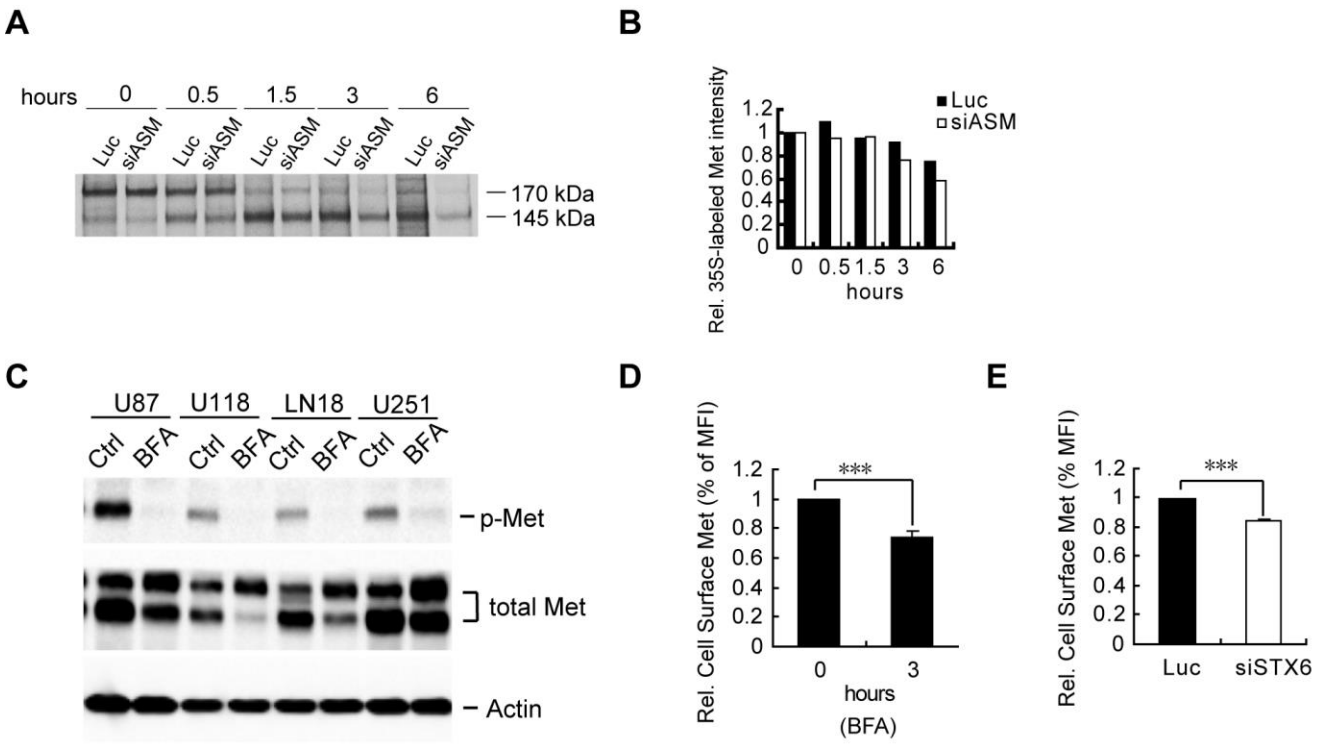

Fig. S3. Effects of Brefeldin A (BFA) and ablation of ASM or STX6 on phosphorylation and intracellular localization of Met. (A) U373-MG cells were transfected with control (Luc) and ASM siRNAs for 72 hours. They were pulse-labeled with ^{35}S-methionine for 1 hour, washed, and chased for various time points in fresh medium without the isotope as indicated. Cells were lysed and Met proteins were immunoprecipitated by anti-MET antibodies, resolved in protein gel, and visualized by fluorography (top panel) and quantified (B). (C) Human glioblastoma U87-MG, U118-MG, LN18, U251-MG cells were treated with or without 3 g/ml BFA for 3 hours. Whole cell lysates were immunoblotted with indicated antibodies, as in Fig. 4F. (D and E) U373-MG cells were treated with or without BFA for 3 hours (D) or transfected with control or STX6 siRNAs for 72 hours (E). Live cells were detached from plates as described in Fig. 2E for FACS analysis. The cells were immunostained with an APC-conjugated anti-Met monoclonal antibody or an isotype mouse IgG control antibody. Cells were then analyzed by FACS method for the surface expression of Met. Results were analyzed by the Student's t test, ***$p<0.001$. Error bars, SD.

Table S1. Antibodies used for immunostaining, immunoprecipitation (IP) and immunoblotting (WB) studies.

Antibodies	Supplier, Catalog Number	Dilution	Uses
SMPD1 (ASM) (mouse)	R&D Systems, MAB5348	1:400	IP
SMPD1 (ASM) (goat)	R&D Systems, AF5348	1:500	WB
Met (mouse, APC-conjugated)	R&D Systems, FAB3582A	1:15	FACS
Control IgG (mouse, APC-conjugated)	R&D Systems, IC002A	1:15	FACS
Syntaxin 6 (sheep, biotinylated)	R&D Systems, BAF5664	1:150	Immunostaining
Met (goat)	R&D Systems, AF276	1:500	IP
Met (rabbit)	Cell Signaling, #8198	1:2000	WB
Met (rabbit, AF488-conjugated)	Cell Signaling, #8494S	1:70	Immunostaining
phospho-Met (Tyr1234/1235)	Cell Signaling, #3077	1:600	WB
phospho-p70 S6K (T389)	Cell Signaling, #9205S	1:1000	WB
phospho-AKT (S473)	Cell Signaling, #4060S	1:1000	WB
p70 S6K (total)	Cell Signaling, #2708S	1:1000	WB
AKT (total)	Cell Signaling, #4691S	1:2000	WB
Syntaxin 6 (rabbit)	Cell Signaling, #2869	1:2000	WB
IGF1R (rabbit)	Cell Signaling, #9750	1:1000	WB
-Actin (mouse)	Cell Signaling, #3700S	1:7000	WB
CD61/integrin 3 (mouse)	BD Biosciences, 555752	1:300	Immunostaining
p230 (mouse)	BD Biosciences, 611280	1:300	Immunostaining
GM130 (mouse)	BD Biosciences, 610822	1:300	Immunostaining
Syntaxin 6 (mouse)	BD Biosciences, 610635	1:300	Immunostaining
LAMP1 (mouse, AF647-conjugated)	BD Biosciences, 562622	1:300	Immunostaining
LAMP2 (mouse, AF647-conjugated)	BD Biosciences, 565305	1:300	Immunostaining

CD63 (mouse, AF647-conjugated)	BD Biosciences, 561983	1:300	Immunostaining
VSVG (rabbit)	Bethyl Laboratories, A190-131A	1:500	IP
GFP (mouse)	Santa Cruz Biotechnology, Sc-9996	1:500	WB
Goat anti-mouse IgG (AF488-conjugated)	Jackson Immunologicals, 115-546-146	1:150	Immunostaining
Goat anti-rabbit IgG (AF488-conjugated)	Jackson Immunologicals 111-546-144	1:150	Immunostaining
Goat anti-mouse IgG (AF647-conjugated)	Jackson Immunologicals 115-606-146	1:300	Immunostaining
Goat anti-rabbit IgG (AF647-conjugated)	Jackson Immunologicals, 115-606-146	1:300	Immunostaining
Streptavidin (Brilliant Violet 421-conjugated)	BioLegend, 405225	1:1000	Immunostaining